Evaluating predictions of ICME arrival at Earth and Mars

Falkenberg, Thea Vilstrup; Taktakishvili, A.; Pulkkinen, A.; Vennerstrøm, Susanne; Odstrcil, D.; Brain, D.; Delory, G.; Mitchell, D.

Published in:
Space Weather

Link to article, DOI:
10.1029/2011SW000682.

Publication date:
2011

Document Version
Publisher's PDF, also known as Version of record

Evaluating predictions of ICME arrival at Earth and Mars

T. V. Falkenberg,[1] A. Taktakishvili,[2] A. Pulkkinen,[2,3] S. Vennerstrom,[1] D. Odstrcil,[2] D. Brain,[4] G. Delory,[4] and D. Mitchell[4]

Received 28 March 2011; revised 4 May 2011; accepted 31 May 2011; published 2 September 2011.

[1] We present a study of interplanetary coronal mass ejection (ICME) propagation to Earth and Mars. Because of the significant space weather hazard posed by ICMEs, understanding and predicting their arrival and impact at Mars is important for current and future robotic and manned missions to the planet. We compare running ENLILv2.6 with coronal mass ejection (CME) input parameters from both a manual and an automated method. We analyze shock events identified at Mars in Mars Global Surveyor data in 2001 and 2003, when Earth and Mars were separated by <80° in heliocentric longitude. The shocks identified at Mars were also identified at Earth, and the majority of the shock sources were identified through the Solar and Heliospheric Observatory–Large Angle and Spectrometric Coronagraph catalogue. We find that arrival times predicted by the two methods at both planets are statistically similar, dynamic pressures predicted when using the automated method are better, and the automated method tends to underestimate both CME width and speed. Using the location of the related flare as the CME direction did not improve results. In addition, changing the CME speed toward the plane-of-sky speed at 20 R_S improves the match to observations, mainly because the speed found by the automated method is underestimated. The time lapse between the shock arrival at Earth and Mars, for the events studied here, is shorter than expected from simulations, and the presence of high speed streams can enable an ICME to arrive almost simultaneously at Earth and Mars. This work will be applied to improve the input parameter methods for ENLIL.

Citation: Falkenberg, T. V., A. Taktakishvili, A. Pulkkinen, S. Vennerstrom, D. Odstrcil, D. Brain, G. Delory, and D. Mitchell (2011), Evaluating predictions of ICME arrival at Earth and Mars, *Space Weather*, *9*, S00E12, doi:10.1029/2011SW000682.

1. Introduction

[2] Interplanetary coronal mass ejections (ICMEs) are one of the most important drivers of space weather. In addition to posing a hazard for near-Earth systems, ICMEs contribute to dramatic changes in interplanetary and planetary radiation environment conditions. Consequently, ICMEs pose a hazard to both manned and robotic planetary missions. Understanding ICME propagation through the solar system, and being able to model this process realistically, is thus important for future spacecraft design, and for possible manned missions. Due to the possible future manned missions to the planet particularly the effects of space weather at Mars are of interest. Understanding the radiation environment at Mars, and in the interplanetary medium between the Earth and Mars, is crucial for mitigating the biological hazard posed by the solar activity.

[3] One heliospheric model providing the possibility of ICME propagation, combined with the background solar wind features, such as high-speed streams and current sheet crossings, is the ENLIL model. The ENLIL version currently available at the Community Coordinated Modeling Center (CCMC) is version 2.6 (ENLILv2.6), which is the model we will use for this study. ENLILv2.6 requires input regarding the CME disturbance (time, location, width, speed, density and temperature) at the model's inner boundary of 21.5 solar radii (R_S). The majority of inputs (time, location, width and speed) can be inferred from the SOHO/LASCO (Large Angle and Spectrometric Coronagraph on board the Solar and Heliospheric Observatory [*Brueckner et al.*, 1995]) 2D images from the C2

[1]National Space Institute, Danish Technical University, Lyngby, Denmark.
[2]NASA Goddard Space Flight Center, Greenbelt, Maryland, USA.
[3]Catholic University of America, Washington, DC, USA.
[4]Space Sciences Laboratory, University of California, Berkeley, California, USA.

or C3 telescope. The STEREO A and B satellites provide stereo images of solar events, providing a more dependable estimate of CME parameters, however not many large scale events have occurred since the launch in October 2006.

[4] Using 2D images to determine parameters of a 3D structure, potentially causes projection effects [*Burkepile et al.*, 2004; *Schwenn et al.*, 2005; *Vršnak et al.*, 2007] and is more efficient in some cases than others. However, 2D SOHO/LASCO images in many cases provide the only available constraints, and are therefore often the basis of techniques developed to determine input parameters for CME models [*Zhao et al.*, 2002; *Michałek et al.*, 2003; *Xie et al.*, 2004; *Pulkkinen et al.*, 2010]. The manual method presented by *Xie et al.* [2004], which builds on the method presented by *Zhao et al.* [2002], has often been used in combination with ENLIL, validating the simulations against near-Earth satellite data [*Taktakishvili et al.*, 2009; *Falkenberg et al.*, 2010; *Vršnak et al.*, 2010] and near-Earth and near-Mars satellite data in combination [*Falkenberg et al.*, 2011]. The method presented by *Pulkkinen et al.* [2010] is an automated method, relying on digital image analysis rather than a manually determined image analysis, giving the advantage of possible fully automated modeling systems.

[5] *Pulkkinen et al.* [2010] compared the input parameters extracted using their technique to those of *Xie et al.* [2004], finding good correspondence, and *Taktakishvili et al.* [2011] compared the effects of the two different input parameter sets when using ENLIL, finding an average error of 6.9 h for the manual method and 11.2 h for the automated method. *Falkenberg et al.* [2011] also compared the performance of the two different input parameter sets in combination with ENLILv2.6 for a study of one event that encountered both Earth and Mars. They found that neither technique adequately predicted the direction of the ICME, inferred directly from the in situ observations at Earth and Mars, but found that the automated method found a better estimation of the initial speed of the CME for the event studied (17 November 2001 halo event).

[6] Generally fast and massive CMEs are related to intense flares [*Yashiro et al.*, 2006; *Vršnak et al.*, 2007], and it is an open question whether the flare location can provide a better estimate of the general direction of the CME than analysis of SOHO/LASCO data. *Falkenberg et al.* [2011] found that the direction of the ICME for a single event was better estimated by the flare location than the direction given by either the *Pulkkinen et al.* [2010] or the *Xie et al.* [2004] method. *Temmer et al.* [2009] also found the location of related flares to be a good estimation of the ICME direction. *Gopalswamy et al.* [2007] presented a statistical study of the geoeffectiveness of halo events at Earth based on their related flare locations. They found that 75% of the disk halos and 60% of limb halos are geoeffective, underscoring the importance of frontside halo CMEs in causing space weather effects and indicating that halo events are very wide. However, finding an accurate estimate of the initial direction of the ICME may not be sufficient for ensuring that propagation models are successful. Recent STEREO observations have shown that ICMEs may be deflected latitudinally, instead of just propagating radially [*Kilpua et al.*, 2009; *Liu et al.*, 2010; *Pomoell et al.*, 2010; *Byrne et al.*, 2010], confirming the results of earlier studies [*Wei and Dryer*, 1991; *Filippov et al.*, 2001; *Cremades et al.*, 2006]. Longitudinal deflections on the order of 30° were also found by *Wang et al.* [2004, 2006] and *Shen et al.* [2009], where fast ICMEs tend to be deflected eastward with the IMF Parker spiral and slower ICMEs are deflected against the IMF Parker spiral. These studies indicate that ICMEs may change direction during propagation, so that assuming radial propagation from their point of origin may not be valid in all cases.

[7] All detected CMEs by SOHO/LASCO are collected in the online SOHO/LASCO catalogue [*Gopalswamy et al.*, 2009; *Yashiro et al.*, 2004], providing the possibility of identifying the CME sources of geoeffective events and events effective at Mars, based on expected travel time to the planets and their estimated initial speeds. The estimated initial speeds in the SOHO/LASCO catalogue are plane-of-sky speeds, however this speed has often been applied in models with good results, assuming that the radial expansion is approximately equal to the lateral expansion close to the Sun [*Gopalswamy et al.*, 2000, 2001; *González-Esparza et al.*, 2003].

[8] In this study we test the input parameter methods presented by *Xie et al.* [2004] and *Pulkkinen et al.* [2010] by running ENLILv2.6 model simulations with the input parameters obtained. We perform simulations of 15 CMEs, based on shock events identified in MGS (Mars Global Surveyor) data at Mars when Earth and Mars are separated by less than 80° heliocentric longitude. We then try to identify the shocks in near-Earth OMNI data if possible. We also perform simulations using the flare locations as indicators of the initial direction of the CME, and estimate for each simulation whether changing the initial speed toward the plane-of-sky speed listed in the SOHO/LASCO catalogue would improve the simulations. We do not aim to achieve the best simulation possible by tweaking of parameters, and only the parameters found from the two techniques are altered, so all remaining parameters outside those found by the input parameter methods (time, direction, width and speed) are kept at their standard values.

[9] Applying multipoint observations in model validation provides a better estimate of the performance of the model, as it is relatively easy to achieve a good reproduction of data at one heliospheric location, while much more difficult to achieve a good reproduction of data at two locations simultaneously [*Falkenberg et al.*, 2011]. We therefore test all the simulations presented in this study against both OMNI data from the near-Earth environment and MGS data at Mars, increasing our ability to estimate the performance of the input parameter method,

Table 1. In Situ Data for the Events Chosen for This Study[a]

	Mars			Earth					
	CME		Particles ER Maximum Background Count Rate	CME				Particles Maximum GOES Signal, >30 MeV	Distance Between Earth and Mars[b] (deg)
	Shock Time (UT)	P_{dyn} Proxy Maximum Value (nPa)		Shock Time (UT)	P_{dyn} Maximum Value (nPa)	Speed Maximum Value (km/s)	Density Maximum Value (cm^{-3})		
Not Identified	**2001/01/19 02:20**	**2.5**	**400**	**2001/01/17 16:25**	**8.5**	**420**	**30**	**0.01**	**73.12**
Event1	2001/04/04 21:40	8	7000	2001/04/04 15:00	9.7	800	11.3	6.5	32.93
Event2	2001/04/12 11:00	10	12,000	2001/04/11 13:40	32	760	38.5	7.5	29.02
Event3	2001/04/19 03:35	2.5	420	2001/04/18 08:35	19.2	535	40	7	26.15
Event4	2001/09/25 19:55	14	95,000	2001/09/25 20:45	39	650	52	38	−36.45
Event5	2001/11/20 03:35	12	2500	2001/11/19 18:15	7.5	622	20	0.2	−55.94
Event6	2001/12/29 06:30	23.6	600	2001/12/29 05:25	25	455	80	1.2	−71.08
Event7	2001/12/31 18:00	7	800	2001/12/30 20:15	9.1	700	8	0.5	−72.34
Event8	2002/01/11 06:45	8.8	10,000	2002/01/10 16:20	10.7	650	18	2	−76.99
Not Identified	**2003/03/19 06:30**	**3**	**250**	**2003/03/17 19:55**	**6**	**840**	**6.5**	**0.02**	**61.48**
Event9	2003/05/29 23:20	20	200	2003/05/29 19:10	64	800	61	2	32.1
Event10	2003/05/31 03:45	8	400	2003/05/30 16:20	23.8	800	25	0.7	31.35
Event11	2003/10/25 09:35	17.5	200	2003/10/24 15:20	36	600	60	0.3	−19.56
Event12	2003/10/30 05:30	21.3	40,000	2003/10/29 06:10[c]	75[c]	2300[c]	18[c]	1030	−21.47
Event13	2003/10/31 11:30	20	2000	2003/10/30 20:00[c]	1[c]	1800[c]	3[c]	100	−21.85
Event14	2003/11/21 04:50	4.5	700	2003/11/20 08:25	19.6	750	28	7.5	−29.83

[a]Data accumulated from the MGS satellite, the OMNI database, and the GOES satellites. Shock times are read from data plots of MGS data and OMNI data. The SOHO/LASCO catalogue was used to try to identify the CME source of the observed shocks (listed in Table 2); the source of the events marked in bold were not identified. The maximum values are the maximum values measured within 12 h of shock arrival.

[b]Heliocentric longitude. Negative distances indicate that Mars was trailing Earth.

[c]Values from the Halloween storm 2003 where there is a gap in the OMNI data; these values are obtained from the reconstructed data shown by *Lopez et al.* [2007, Figure 1].

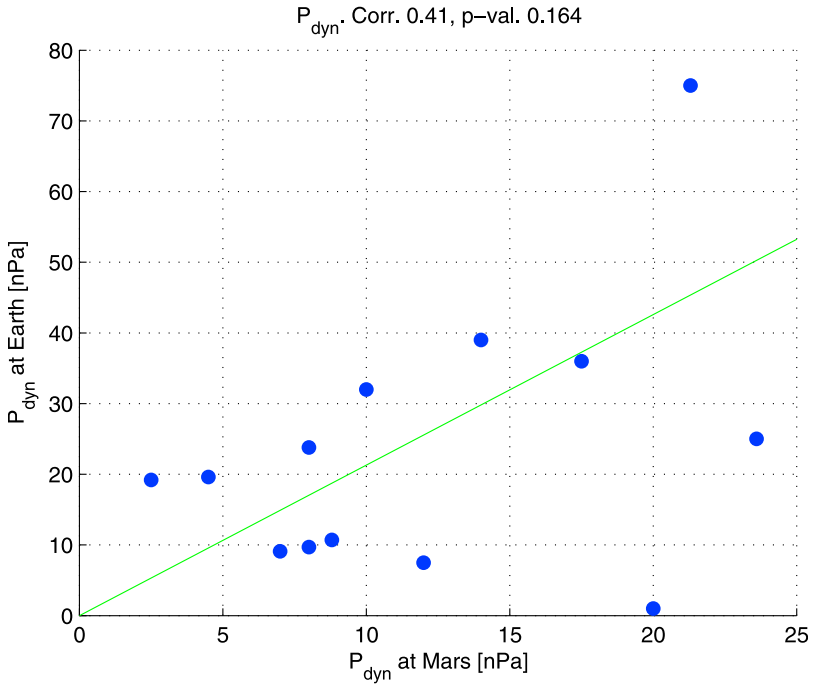

Figure 1. The maximum dynamic pressure measured by satellites near Earth during ICME arrival against the maximum value of the pressure proxy measured by MGS at Mars. Green line indicates $1/r^2$ propagation of the dynamic pressure at Earth to Mars (i.e., scaling the density by $1/r^2$), as found by *Vennerstrom et al.* [2003] and *Crider et al.* [2003] for times of quiet solar wind. The value of r used is 1.45 AU. Values are listed in Table 1. "Corr" is the correlation coefficient of the points, and "p-val" is the probability of achieving the same correlation coefficient for randomly distributed points.

and allowing us to perform statistics on shock events encountering both Mars and Earth.

2. Event List

[10] Our event list is based on ICME events identified at Mars from MGS data, when Earth and Mars were separated by less than 80° in heliocentric longitude. MGS operated in a continuous mapping orbit from 1999 to 2006. For this study we concentrate on events identified in 2001 and 2003 (Table 1). In order to identify an ICME event, we look for shock signatures in both the magnetometer data and the background particle data from the Electron Reflectometer (ER) on MGS.

[11] The magnetometer data is converted to magnetic pressure by first estimating the magnetic field intensity at the subsolar point, in the manner described by *Brain et al.* [2005], and then converting from magnetic field intensity, B, to pressure (P_{mag}) by using $P_{mag} = \frac{B^2}{2\mu_0}$ (where μ_0 is the vacuum permeability given by $4\pi \cdot 10^{-7}$ H m^{-1}). The magnetic pressure is then assumed to be a proxy for the solar wind dynamic pressure, P_{dyn}. The validity of the pressure proxy relies on pressure conservations throughout the Martian system (demonstrated by *Dubinin et al.* [2008]), and the magnetic pileup region being dominated by magnetic pressure and the solar wind being dominated by dynamic pressure. This assumption appears to be valid during quiet times [*Vennerstrom et al.*, 2003; *Crider et al.*, 2003], but it has also been used for ICMEs with credible results [*Falkenberg et al.*, 2011]. Figure 1 shows the maximum obtained values for dynamic pressure at Mars for the events treated here, against the maximum values measured near Earth for the same events. This indicates that the Martian pressure proxy is in fact a reasonable estimate of the dynamic pressure in the solar wind, and is at least of the correct order of magnitude. The magnetic intensity at the subsolar point (and therefore the pressure proxy) is calculated once per orbit of MGS around Mars, with a resulting cadence of about 2 h.

[12] The ER instrument, though meant to measure electrons, is penetrated by solar energetic particles above ~30 MeV, giving rise to high background levels in the instrument data [*Brain*, 2006; *Brain et al.*, 2011; *Falkenberg et al.*, 2011]. We use the ER data from the three highest energy channels (~11, 14 and 18 keV) as indicators of the background count rate. A shock front, if present, is evident as a sudden increase in this count rate caused by Solar Energetic Particles (SEPs) arriving with the shock.

[13] We define a shock at Mars as a simultaneous jump in the pressure proxy of at least 2 nPa and at least 50 in the ER background count rate. Using these criteria 16 shocks events were found at Mars during the periods in 2001 and 2003 when Earth and Mars were separated by less than 80° in heliocentric longitude. These are listed in Table 1. These events were then identified at Earth, if possible, by searching for shocks in OMNI velocity and density data and GOES particle data within 1.5 days before the shock arrival at Mars (also listed in Table 1). The OMNI data, provided and maintained by NASA Goddard Space Flight Center's National Space Science Data Center, is composed of ACE, WIND and Geotail (in the periods analyzed here) satellite data. The dynamic pressure at Earth is calculated from the velocity and density satellite data using $P_{dyn} = N * m_p * v^2$, where N is the number density, m_p is the proton mass and v is the velocity. The ratio of helium in the number density is not taken into consideration. All values are read manually from data plots.

[14] We then used the SOHO/LASCO catalogue [*Gopalswamy et al.*, 2009; *Yashiro et al.*, 2004] to identify the CME source of the observed shocks (listed in Table 2), sometimes obtaining multiple candidates for each shock. 21 CMEs were found, hereunder 14 halo CMEs, 5 partial halo (p.halo) CMEs and two nonhalo CMEs. 20 of 21 CMEs have assumably related flares. The source of two of the shock events from Table 1 could not be identified and are marked in grey. The CMEs in Table 2 were then modeled using ENLILv2.6, applying two different methods for finding input parameters, described in section 4. These input parameter methods only work under certain conditions, i.e., halo CMEs and fairly isolated CME events, and the events marked in grey in Table 2 could therefore not be modeled. This left only 13 identified shocks at Mars and a total of 15 CMEs to be modeled, i.e., Events 1 through 8 and 10 through 14 in Table 1.

3. ENLILv2.6

[15] The ENLIL model is available for online runs at the Community Coordinated Modeling Center (CCMC) at NASA Goddard Space Flight Center. ENLIL [*Odstrcil and Pizzo*, 1999; *Odstrcil et al.*, 2004] is a 3D time-dependent MHD solar wind model, capable of propagating features, representing CMEs, in a cone-like manner through a realistic model of the solar wind. ENLIL can be run without a CME or with up to 5 CMEs in one run, which spans one Carrington Rotation (CR). As input for the background solar wind ENLIL uses output from either the Magnetohydrodynamics Around a Sphere (MAS [*Riley et al.*, 2006]) or the Wang-Sheely Arge (WSA [*Arge and Pizzo*, 2000]) model. MAS is a full 3D MHD model of the corona and WSA uses both a combination of potential field and current sheet models. Both takes input from magnetograms, giving the features of the background solar wind at the inner boundary of ENLIL, namely 21.5 solar radii (R_S). For this study we used ENLIL version 2.6 (ENLILv2.6) available at CCMC. This is a slightly simplified version of the full ENLIL model. We ran the model with input from the WSA version 1.6 using Mount Wilson Observatory (MWO) magnetograms. For a few CRs, namely 1975 and 1984, this information was not available and the model was run using the MAS model instead, affecting events 3, 6 and 7 in Table 2. MAS uses synoptic magnetograms from the National Solar Observatory (NSO) as input. All the runs performed for this study are available through the CCMC Web site at ccmc.gsfc.nasa.gov.

[16] ENLIL has previously been verified against data recorded near-Earth [*Falkenberg et al.*, 2010; *Taktakishvili et al.*, 2009, 2011; *Lee et al.*, 2009], and does quite well at predicting arrival times and major solar wind parameters near-Earth. A detailed event study was also previously performed, by *Falkenberg et al.* [2011], using the ENLILv2.6 model and verifying it against data from both Mars and Earth.

[17] The input parameters for the CME in ENLILv2.6 are those of time, speed, density, temperature, direction and angular width. ENLILv2.6 does not include a magnetic cloud in the CME (see *Falkenberg et al.* [2010] and *Taktakishvili et al.* [2010] for an extensive description of input parameters and their effects on the model). The majority of these inputs (i.e., time, speed, direction and angular width) can be inferred from SOHO/LASCO images in two different ways described in section 4. The standard values were used for the remaining ICME input parameters, namely 1200 cm^3 for density and $0.8 \cdot 10^6$ K for temperature.

4. Methods of Finding Input Parameters for ENLILv2.6

[18] There are two main methods of finding input parameters for the CME disturbance fed into ENLIL, based on SOHO/LASCO images from the C3 coronograph. A manual method presented by *Xie et al.* [2004], which was used, e.g., by *Falkenberg et al.* [2010, 2011] and *Taktakishvili et al.* [2009], and a newer, automated method described by *Pulkkinen et al.* [2010], which was used by *Falkenberg et al.* [2011] and *Taktakishvili et al.* [2011]. These are described in more detail below.

4.1. Manual Method

[19] We refer to the method presented by *Xie et al.* [2004], as the manual method, where consecutive SOHO/LASCO images are used to infer the time, width, direction and speed of a CME. Using two SOHO/LASCO C3 white-light running difference images, ellipses are drawn around the outline of the CME. The CME shows up as a large white expanding structure. The ellipses are drawn as to contain the entire area assumably related to the CME, and so that at least one axis of the ellipse passes through the center of the Sun [see *Xie et al.*, 2004, Figure 4]. A perfect cone is then fitted to these ellipses, based on the assumption that the CME will propagate and expand in a cone-like manner, providing speed, direction and width at any given

Table 2. CMEs Identified as the Source of the Events Chosen for This Study[a]

	CME						Flare				
	Date	First Appearance in LASCO/C2	Calculated Onset	LASCO Width	LASCO Initial Speed	LASCO Speed at 20 R_{Sun}	Flare Start	Flare Class	Flare Location	Active Region	Heliocentric Longitudinal Distance Between Earth and Mars (deg)
Event1a	2001-04-01	11:26	10:59	Halo	1475	1549	10:55	M5.5	E90S22[b]		32.93
Event2a	2001-04-09	15:54	15:22	Halo	1192	1198	15:20	M7.9	W04S21[c]	9415	29.02
Event2b	2001-04-10	05:30	05:16	Halo	2411	2974	05:06	X2.3	W09S23[c]	9415	28.54
Event3a	2001-04-15	14:06	13:22	245 p.Halo	1199	1064	13:19	X14.4	W85S20	9415	26.15
Event4a	2001-09-24	10:30	10:16	Halo	2402	2500	09:32	X2.6	E23S16[c]	9632	–36.45
Event5a	2001-11-17	05:30	04:41	Halo	1379	1350	04:49	M2.8	E42S13[c]	9704	–55.94
Event6a	2001-12-25	11:30	10:53	Halo	1773	1778	11:30	C5.4	W48N11[d]	9751	–71.08
Event6b	2001-12-26	05:30	04:58	281 p.Halo	1446	1295	04:32	M7.1	W54N08	9742	–71.50
Event7a	2001-12-28	20:30	20:02	Halo	2216	2226	20:02	X3.4	E90S24[b]		–72.34
Event8a	2002-01-08	17:54	17:41	Halo	1794	1977	17:13	C7.2	W42S18[d]	9767	–76.99
Event9a	**2003-05-27**	**22:06**	**21.36**	**215 p.Halo**	**1122**	**1122**					**32.10**
Event9b	**2003-05-27**	**23:50**	**22:44**	**Halo**	**964**	**908**	**22:56**	**X1.3**	**W17S07[c]**	**10365**	**32.10**
Event10a	**2003-05-28**	**00:50**	**00:13**	**Halo**	**1366**	**1414**	**00:17**	**X3.6**			**31.72**
Event10b	**2003-05-28**	**04:26**	**03:57**	**212**	**1210**	**1171**	**04:43**	**C7.6**			**31.72**
Event10c	**2003-05-28**	**14:06**	**13:44**	**113**	**1283**	**1319**	**13:50**	**C1.3**			**31.72**
Event10d	2003-05-29	01:27	00:36	Halo	1237	1184	00:51	X1.2	W37S06[c]	10365	31.35
Event11a	2003-10-23	08:54	08:16	53 p.Halo	1406	1350	08:19	X5.4	E88S21	10486	–19.56
Event12a	2003-10-28	11:30	11:01	Halo	2459	2268	09:51	X17.2	E08S16[c]	10486	–21.47
Event13a	2003-10-29	20:54	20:35	Halo	2029	1519	20:37	X10	W02S15[c]	10486	–21.85
Event14a	2003-11-18	08:50	08:05	Halo	1660	1656	08:12	M3.9	E18N00[b]	10501	–29.83
Event14b	**2003-11-18**	**09:50**	**09:37**	**95 p.Halo**	**1824**	**1941**	**09:23**	**M4.5**			**–29.83**

[a]Data accumulated from the SOHO/LASCO and GOES X-ray catalogues. Calculated onset of the CME is from the SOHO/LASCO catalogue through the VSO interface (vso.nso.edu). When no flare location or active region is listed, it is not available in the GOES X-Ray catalogue. The CMEs are numbered according to which event from Table 1 they are assumably related to. The events marked in bold are the events we were not able to find input parameters for and therefore have not modeled. Negative heliocentric longitudinal distances indicate that Mars was trailing Earth.

[b]Locations found by *Gopalswamy et al.* [2007].

[c]Locations confirmed by *Gopalswamy et al.* [2007].

[d]Locations according to *Gopalswamy et al.* [2007] that are not related to the CME.

Table 3. Input Parameters for ENLILv2.6 for the CMEs from Table 2 Found Using the Methods Described in Section 4[a]

	SOHO/LASCO Catalogue		Automated Method at 21.5 R_S					Manual Method at 21.5 R_S				
	Date	Time (UT)	Speed (km/s)	Start Time (UT)	Speed (km/s)	Longitude (deg)	Latitude (deg)	Width (deg)	Start Time (UT)	Speed (km/s)	Longitude (deg)	Latitude (deg)	Width (deg)
Event1a	2001-04-01	11:26	1475	14:06	1281 ± 273	−20 ± 4	−3 ± 1	32 ± 6	13:58	1750	−33	−14	50
Event2a	2001-04-09	15:54	1192	19:17	1009 ± 298	3 ± 1	−10 ± 3	36 ± 7	19:55	895	19	−12	72
Event2b	2001-04-10	05:30	2411	07:55	1273 ± 277	6 ± 2	−14 ± 3	38 ± 6	07:43	1638	25	−23	71
Event3a	2001-04-15	14:06	1199	17:07	1180 ± 279	0 ± 1	0 ± 0	49 ± 6	17:07	1232	31	−11	50
Event4a	2001-09-24	10:30	2402	13:13	1390 ± 299	−26 ± 5	−7 ± 2	48 ± 6	12:06	3227	−31	−21	68
Event5a	2001-11-17	05:30	1379	08:08	1142 ± 292	−14 ± 4	10 ± 2	34 ± 6	06:42	844	−19	10	31
Event6a	2001-12-25	11:30	1773	13:33	1467 ± 307	1 ± 0	−17 ± 3	33 ± 5	13:49	1420	−23	−31	70
Event6b	2001-12-26	05:30	1446	08:27	1002 ± 304	23 ± 8	−3 ± 1	31 ± 7	08:02	1791	48	8	51
Event7a	2001-12-28	20:30	2216	00:24[b]	917 ± 264	−40 ± 12	−15 ± 4	58 ± 8	23:22	1691	−34	−26	62
Event8a	2002-01-08	17:54	1794	19:37	1170 ± 242	−12 ± 3	1 ± 0	30 ± 5	20:46	1213	−43	12	55
Event10d	2003-05-29	01:27	1237	04:36	875 ± 267	6 ± 3	0 ± 0	32 ± 7	04:54	1121	54	1	59
Event11a	2003-10-23	08:54	1406	11:24	1254 ± 244	−22 ± 5	2 ± 1	30 ± 5	12:09	975	−37	3	51
Event12a	2003-10-28	11:30	2459	13:44	1419 ± 291	0 ± 1	1 ± 1	48 ± 5	12:49	2868	41	7	83
Event13a	2003-10-29	20:54	2029	23:28	1349 ± 297	4 ± 1	−5 ± 1	43 ± 5	23:10	1390	7	−9	84
Event14a	2003-11-18	08:50	1660	11:25	1233 ± 303	5 ± 2	−10 ± 3	41 ± 7	11:28	1193	37	−29	71

[a]Plus-or-minus sign indicates standard deviation of the parameter distribution found using a bootstrap method for the automated method. Longitude 0 and latitude 0 are toward Earth. Negative longitudes and latitudes correspond to east and south in flare coordinates, respectively. The width listed is cone half-angle width.
[b]This is the time the following day.

point. The method estimates the radial speed of the CME, calculated by using the time stamps of the running difference images.

[20] This method is exclusive to halo and partial halo CMEs as the CME is needed to expand on both sides of the Sun in the SOHO/LASCO C3 images. The method also requires ellipses rather than circles, as the solution will not be unique if circles are drawn. This artificially excludes the possibility that a CME originated at W00N00. The drawing of the ellipses is also highly subjective as it depends on the users estimate of what features are related to the CME.

[21] The input parameters obtained from the manual method are listed in Table 3. In this study, all the manual method parameters were extracted by A. Taktakishvili for consistency with the studies presented by *Taktakishvili et al.* [2009] and *Pulkkinen et al.* [2010]. All parameters were extracted at the location of the inner boundary of ENLILv2.6, i.e., 21.5 R_S.

4.2. Automated Method

[22] We refer to the method presented by *Pulkkinen et al.* [2010] as the automated method. It also builds on consecutive SOHO/LASCO images to infer time, width, direction and speed of a CME, but here the analysis is done automatically and is therefore independent of the person performing the analysis. At least two SOHO/LASCO C3 white-light running difference images are put through an image analysis routine [see *Pulkkinen et al.*, 2010, Figure 2], in which (1) the contrast of the image is adjusted (added) by linearly mapping the original values to values covering the full gray scale intensity range, (2) the image is filtered using a median filter, and (3) the pixels of the filtered image are converted into binary values based on a threshold. Pixels brighter than 70% of the intensity maximum are assigned as being part of the CME. These points are then used to find the fit for the conic CME approximation. All detected CME data points are used and equal weight is given to all data points. The inversion scheme described by *Pulkkinen et al.* [2010, equations 3 and 5] is then used to find the conic parameters. It is noted that we use an updated version of the algorithm described by *Pulkkinen et al.* [2010]. This modified version will be documented in detail in another manuscript under preparation. The new approach is less likely to get stuck in local minima as the optimization progresses. By applying a bootstrap method, the automatic approach also provides probability distributions of the solutions giving one a measure of the confidence with which the parameters should be applied.

[23] This method is again exclusive to halo and partial halo CMEs. To provide unique solutions also in cases when CMEs is originating at W00N00 the automatic method uses climatological opening angles to weigh the solution obtained from the inversion. It should be noted that the method used to extract the area of the CME cannot distinguish between simultaneously occurring CME events. Consequently, only single isolated CME

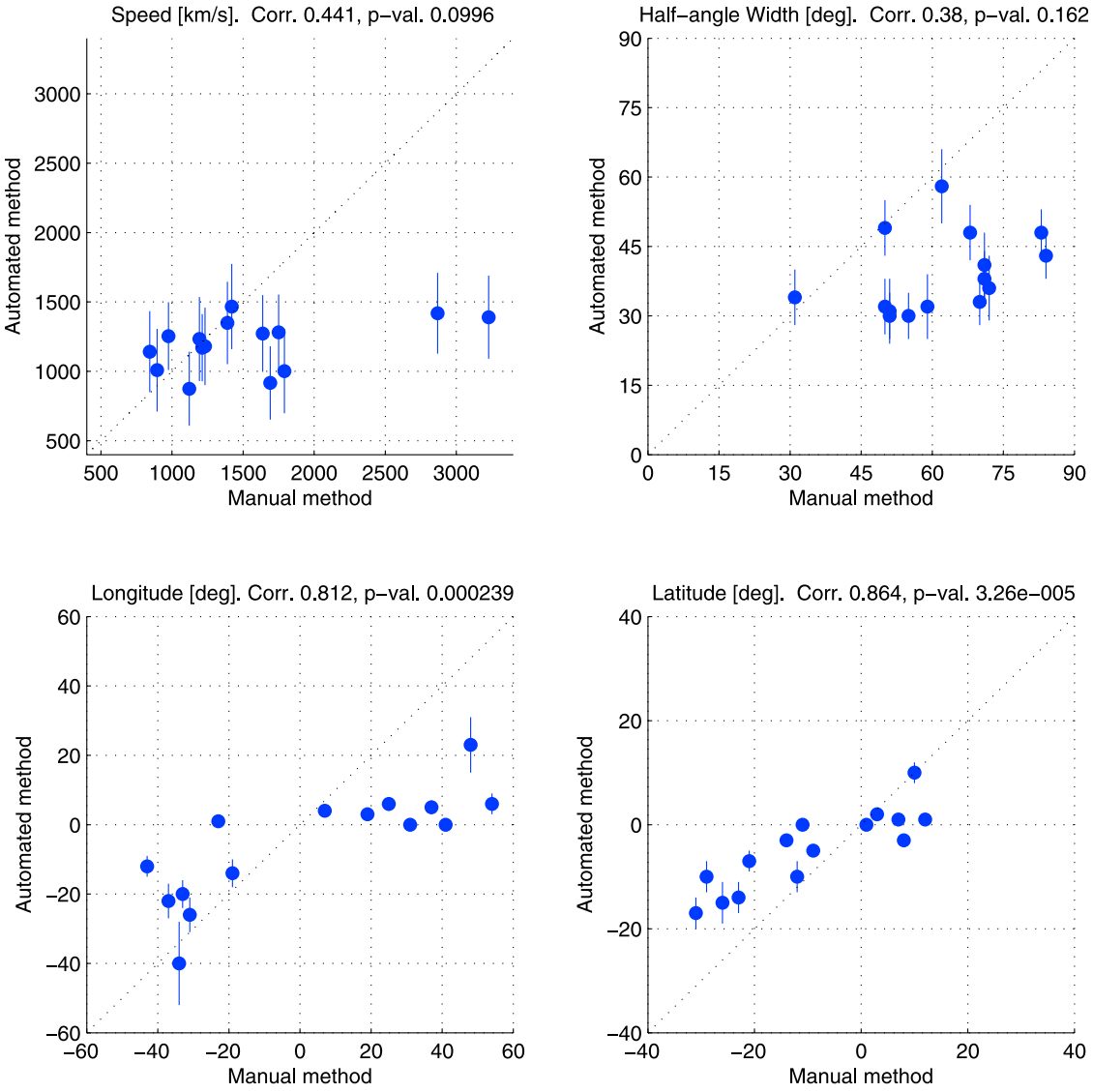

Figure 2. Comparison of the input parameters listed in Table 3 in the same format as *Pulkkinen et al.* [2010, Figure 4] for easy comparison. "Corr" is the correlation coefficient of the points, and "p-val" is the probability of achieving the same correlation coefficient for randomly distributed points.

events can be treated. The input parameters are listed in Table 3. All parameters were extracted at the location of the inner boundary of ENLILv2.6, i.e., 21.5 R_S.

4.3. Comparison of Parameters

[24] The parameters found using the two methods presented above are listed in Table 3 and compared in Figure 2. The most obvious and systematic differences between the two input parameter methods are that the width found by the automated method is generally less than that found by the manual method, and that the speed is typically lower, especially for fast events. Also these two parameters are not correlated (correlation coefficients 0.44 and 0.38, seen in Figure 2). The smaller width found by the automated method is understandable as the manual method uses ellipses surrounding the entire outline of the CME while the automated method uses the cross-sectional area. However, results for the automated method using the CME outline instead of the cross-sectional area to determine the width, did not remove this effect. This difference was also found by *Pulkkinen et al.* [2010] and they argued that the values found by the automated method may be more realistic. The discrepancy in speed was not found by *Pulkkinen et al.* [2010], however they also had one event which was found to be almost 3000 km/s by the manual method and just over 2000 km/s by the automated method. For the events chosen here we have two such events found to have an initial speed of just over and just under

3000 km/s by the manual method and around 1500 km/s by the automated method. Disregarding these two CMEs, the remaining speeds do not differ significantly but the values found by the manual method are still slightly and systematically higher. The speeds found by the manual method range from 844 km/s to 3227 km/s, while the speed found by the automated method range from 875 (±267) km/s to 1467 (±307) km/s. The longitude and latitude positions found by the automated method are typically closer to 0 than the values found by the manual method, perhaps because the automated method does not artificially force CMEs origins away from W00N00 as discussed by *Pulkkinen et al.* [2010]. Overall, Figure 2 looks remarkably similar to *Pulkkinen et al.* [2010, Figure 4] and *Taktakishvili et al.* [2011, Figure 1], with the exception of the velocity comparison by *Taktakishvili et al.* [2011], where the range of velocities found using the automated method is much broader. Also the correlation between the widths found is much better here, perhaps due to the improvement of the automated method by applying stochastic tunneling.

5. Results and Discussion

[25] We compare simulations and data by comparing two basic parameters at each planet, namely arrival time of the ICME shock front and the maximum dynamic pressure reached during the ICME passing. At Earth we also compare the maximum speed and density during the event, however at Mars we only have a proxy for the total solar wind dynamic pressure. We use the MGS data at Mars and the OMNI and GOES data near-Earth, as described in section 2. Simulations where the ICME does not encounter one planet are not included in the statistics for that planet. As the half-angle widths found by the automated method are generally more narrow than those found by the manual method, the simulations done with the parameters found by the automated method are less likely to encounter either planet.

[26] It should be noted that the purpose of this study is not to obtain the best ENLILv2.6 simulation possible, and that all the runs here could be improved by fine-tuning the background conditions and the input parameters [see, e.g., *Falkenberg et al.*, 2011] for Event 5, *Falkenberg et al.* [2010], and *Taktakishvili et al.* [2010]). Our purpose is only to asses the two input parameter methods presented in section 4 against each other. For this reason all remaining parameters aside from the parameters found by the two methods, and the magnetogram used for the specific time period, were left to their standard values used by the CCMC.

[27] From the event list (section 2) we see that all of the shock events identified at Mars in the periods in 2001 and 2003 when Mars and Earth are separated by less than 80° in heliocentric longitude, are caused by fast halo or partial halo events (Table 2), with the exception of Events 10b and 10c which are however still wide and fast events. We also see that all of the shock events identified at Mars in these periods could be associated with a shock event at Earth (Table 1).

[28] The events marked in grey in Table 1 that could not be identified in the SOHO/LASCO catalogue are the only two events with more than 24 h separating the shock arrival at Earth and at Mars. They are also the two weakest particle shock events at Earth, and among the weakest for both dynamic pressure, speed and density (Table 1). This implies that these were not halo events seen from Earth, and may explain why the source of the shock is not evident in the SOHO/LASCO catalogue. It is however surprising that the time lapse between the shock arrival at Earth and Mars is the largest for these two events, as it seems that these were events which hit Mars full on and only grazed Earth. Assuming a smooth, curved shock front, the time lapse between the shock arrival at the two planets should have been relatively small [*Falkenberg et al.*, 2011].

5.1. Applying Parameters From the Two Input Parameter Methods

[29] The simulation results using the parameters from Table 3 are listed in Table 4 together with the satellite data for both planets, so the data and the two simulations are easily compared for each event. The overall results show that while the simulation results in some cases are very close to the satellite data for one or both planets, others are much further off. There is no clear tendency for one input parameter method to yield better results than the other, and in some cases the results of the two simulations are very similar. Event 1 fails to encounter Mars for both simulations, while Event 6 and 8 fails to encounter Mars only when using the automated method. Both input parameter methods find Event 1 to be an eastern event (E33 for the manual method and E20 for the automated method), while we know Mars was leading Earth by 33° (Table 1) and is therefore more likely to be hit by a western event. Earth and Mars are separated by ~71° during Events 6a and 6b, but the automated method predicts half-angle widths of only 33° and 31°. It would therefore not be possible for the ICMEs in Event 6 to encounter both Mars and Earth when using the automated method. The propagation direction found for Event 8 by the two methods was very different (i.e., in corresponding CME origin notation; E43N12 for the manual method and E12N01 for the automated method), and the automated method indicates a much narrower ICME (half-angle width 30°) than the manual method (half-angle width 55°). As Mars was trailing Earth by almost 77° in heliocentric longitude (Table 1) it is not surprising that the ICME in the simulation using the parameters from the automated method fails to encounter Mars.

[30] Event 10 is not well replicated with either input parameter method; the ICME arrived late at both planets. This is likely due to the fact that only Event 10d was simulated, and not Events 10a, 10b and 10c (Table 2). An ICME traveling in the wake of other fast and massive ICMEs is likely to travel faster, as the solar wind has been depleted of particles that were swept up by the previous

Table 4. Results of the Simulations Using the Parameters Listed in Table 3[a]

	Mars		Earth			
	Arrival Time (UT)	P_{dyn} (nPa)	Arrival Time (UT)	P_{dyn} (nPa)	Speed (km/s)	Density (cm^3)
Event1 data	2001/04/04 21:40	8	04/04 15:00	9.7	800	11.3
Event1 man			04/03 12:00	20	570	38
Event1 auto			04/04 08:24	11	420	39
Event2 data	2001/04/12 11:00	10	04/11 13:40	32	760	38.5
Event2 man	2001/04/12 12:28	72	04/11 14:09	355	1080	191.5
Event2 auto	2001/04/13 02:24	25.1	04/11 20:09	208	840	191
Event3 data	2001/04/19 03:35	2.5	04/18 08:35	19.2	535	40
Event3 man	2001/04/19 04:48	24	04/17 19:55	79	534	166
Event3 auto	2001/04/19 09:36	19	04/17 18:14	105	573	192
Event4 data	2001/09/25 19:55	14	09/25 20:45	39	650	52
Event4 man	2001/09/26 03:50	48	09/25 19:40	118	760	122
Event4 auto	2001/09/27 13:12	17	09/27 00:00	27	455	80
Event5 data	2001/11/20 03:35	12	11/19 18:15	7.5	622	20
Event5 man	2001/11/21 22:19	2	11/19 14:24	12.5	550	25
Event5 auto	2001/11/21 16:48	2.2	11/19 05:45	26.4	650	37.5
Event6 data	2001/12/29 06:30	23.6	12/29 05:25	25	455	80
Event6 man	2001/12/27 17:31	49	12/27 07:12	152	1000	205
Event6 auto			12/27 12:00	61.5	730	142
Event7 data	2001/12/31 18:00	7	12/30 20:15	9.1	700	8
Event7 man	2001/12/31 04:04	22	12/30 03:36	192	1000	120
Event7 auto	2002/01/01 06:00	16	12/30 20:24	109.5	760	139
Event8 data	2002/01/11 06:45	8.8	01/10 16:20	10.7	650	18
Event8 man	2002/01/11 20:09	6.58	01/10 09:36	31.3	900	23
Event8 auto			01/10 08:24	30.8	900	23
Event10 data	2003/05/31 03:45	8	05/30 16:20	23.8	800	25
Event10 man	2003/06/01 00:57	17	05/31 05:45	27	635	41
Event10 auto	2003/06/01 19:40	6.5	05/31 07:12	22	620	37
Event11 data	2003/10/25 09:35	17.5	10/24 15:20	36	600	60
Event11 man	2003/10/26 16:48	8	10/25 19:12	14	540	30
Event11 auto	2003/10/26 13:12	5.7	10/25 18:00	10	500	23
Event12 data	2003/10/30 05:30	21.3	10/29 06:10	56.6	2300	18
Event12 man	2003/10/30 02:24	42	10/29 11:31	240	1250	102
Event12 auto	2003/10/31 03:36	20	10/30 05:16	60	700	75.5
Event13 data	2003/10/31 11:30	20	10/30 20:00	5.4	1800	1
Event13 man	2003/10/31 22:48	17.8	10/31 11:02	90	1150	50
Event13 auto	2003/11/01 07:12	5	10/31 11:16	33	985	26
Event14 data	2003/11/21 04:50	4.5	11/20 08:25	19.6	750	28
Event14 man	2003/11/23 02:24	5.5	11/20 08:38	18.4	740	20
Event14 auto	2003/11/22 16:48	5	11/20 09:07	14	700	18

[a]Listed for each event simulated is the satellite data and the results using the manual method and the automated method. The parameters listed are the arrival time at both Mars and Earth as well as the maximum dynamic pressure seen during the ICME arrival; for Earth the maximum speed and density are also given. When no data is listed the simulated ICME did not encounter the planet.

ICME, and the following ICME will therefore experience less drag. Event 10d does not experience this effect in the simulations presented here, due to the fact that input parameters could not be found for Events 10a, 10b and 10c with either input parameter method. *Jackson et al.* [2008] presents a study of the 27 and 28 May 2003 CMEs (i.e., Events 10a, 10b, 10c and some additional smaller nonhalo CMEs at this time) using SMEI (Solar Mass Ejection Imager) data to reconstruct the ICME masses, indicating that these were the responsible events for the shock seen on 30 May at Earth and not event 10d, however they also note that all of these ICMEs merge as the later CMEs have larger initial speeds than the preceding ones.

[31] In order to get a better picture of how the results obtained using the two methods compare, the deviations in arrival time and dynamic pressure between the simulations and the satellite data are shown in Figure 3. The results for arrival time at both planets are similar for the two methods, but the range of values in the dynamic pressure deviation, as well as the error in dynamic pressure prediction, is larger for the manual method at both planets. Also the simulation using the manual method parameters arrive earlier. There is also a linear correlation between the dynamic pressure found by simulations with the manual method parameters and the automated method parameters at both planets. This tendency is most pronounced at Earth: in fact, the correlations are 90.7% for Mars and 98.3% for Earth, but the slope of the tendency is above 1, indicating that the dynamic pressure found using the manual parameters is systematically higher. The event with very bad dynamic pressure determination at Earth, for both methods, is Event 13, i.e., the second Halloween 2003 CME. For this ICME we have no satellite data at Earth and the satellite data used is that reconstructed by

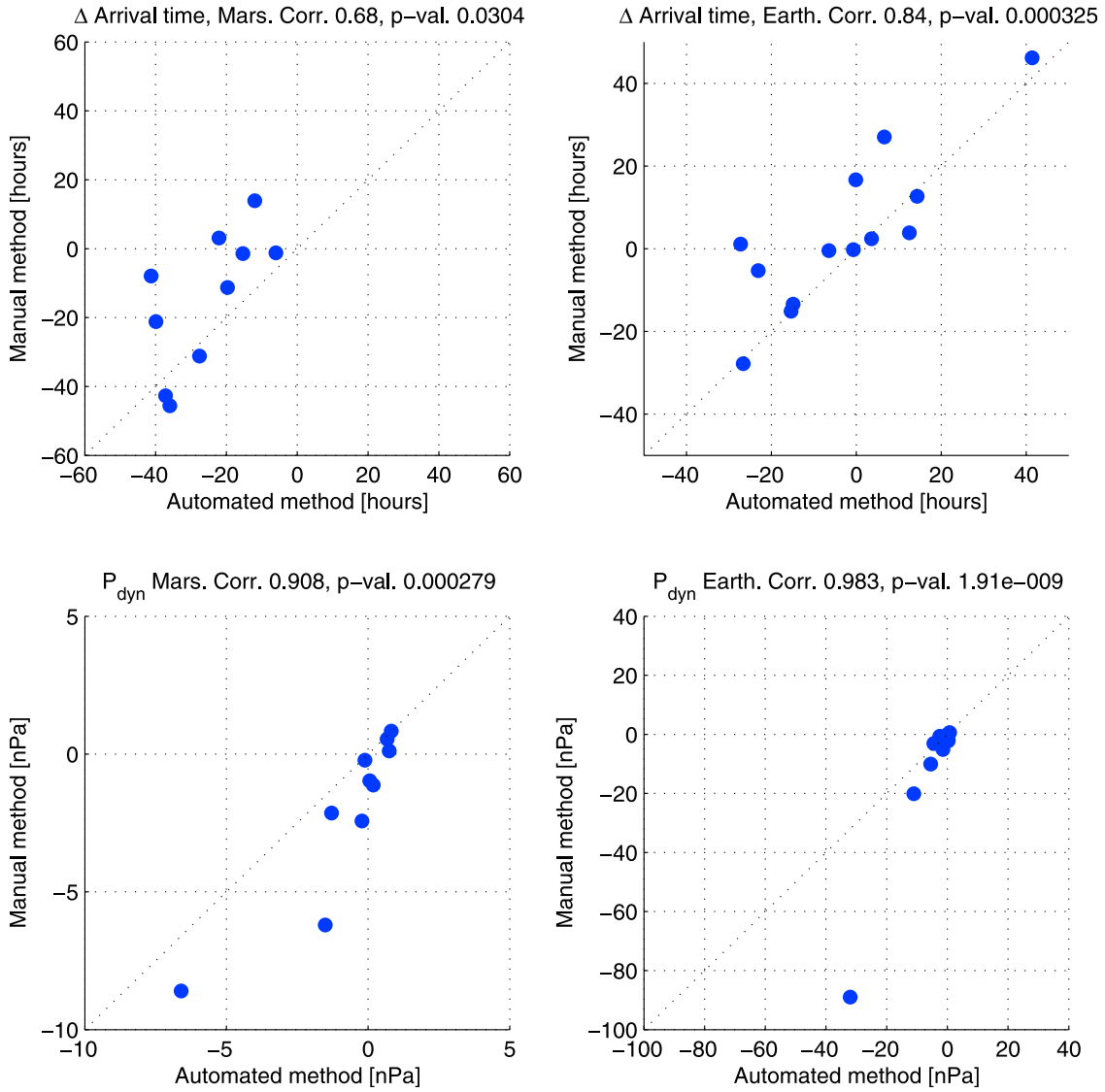

Figure 3. The deviation (top) in arrival time and (bottom) in the maximum P_{dyn} reached during the ICME arrival for (left) Mars and (right) Earth for the two input parameter methods using the parameters listed in Table 3. Δ arrival time is calculated as data minus model, ergo negative values indicate that the event arrived later in the simulation than in the satellite data. The deviation in P_{dyn} is calculated as data minus model divided by data, ergo a value of –5 means the dynamic pressure was overestimated by 5 times in the simulation in relation to the satellite data. "Corr" is the correlation coefficient of the points, and "p-val" is the probability of achieving the same correlation coefficient for randomly distributed points.

Lopez et al. [2007]. In this reconstruction there is almost no density for this second ICME shock arrival, and the dynamic pressure estimated is therefore very low (1 nPa), which may be because of bad reconstruction of the data, or because this event is a special case, since it is a very large event following another very large event. The model results for this event should therefore not be given too much weight.

[32] The average and average absolute error of the values from Figure 3 are listed in Table 5. Here we see that while simulations with parameters from both methods generally arrive too late at Mars, the simulations with the automated method parameters generally arrive too late at Earth also, while the simulations with the manual method parameters arrive too early at Earth. This corresponds to the results of *Taktakishvili et al.* [2009, 2011] for the manual method at Earth. While the arrival time error is comparable using

Table 5. Average and Average Absolute of the Values Plotted in Figure 3 as Well as Average and Average Absolute Error of the Density and Speed at Earth[a]

		Average Error		Average Absolute Error	
	Type	Mars	Earth	Mars	Earth
Arrival time (h)	Manual	−10.166	3.645	19.166	13.253
	Automated	−23.374	−2.779	23.374	14.840
P_{dyn}	Manual	−1.752	−10.364	2.042	10.467
	Automated	−0.657	−4.416	1.110	4.660
Speed	Manual		−0.081		0.319
	Automated		0.084		0.283
Density	Manual		−6.188		6.309
	Automated		−4.366		4.516

[a]Results of using the parameters from Table 2. P_{dyn}, speed, and density are determined by data minus model divided by data.

the two different input parameter methods, the dynamic pressure determination is better when using the automated method, at both planets, though more significantly at Earth. The absolute error in arrival time of ~13.3 h at Earth for the manual method is double the 6 h average absolute error found by *Taktakishvili et al.* [2009], and the 6.9 error found by *Taktakishvili et al.* [2011]. Also the absolute error in arrival time of ~14.8 h at Earth for the automated method is worse than the 11.2 h found by *Taktakishvili et al.* [2011]. It should be noted that *Taktakishvili et al.* [2009] used an earlier version of ENLIL and *Taktakishvili et al.* [2011] used an earlier version of the automated method, without the stochastic tunneling. It should also be noted that while *Taktakishvili et al.* [2009] analyzed nice, easily analyzed halo events only, and *Taktakishvili et al.* [2011] also analyzed only strong halo events, we have here analyzed a set of events which were not picked because of the clarity of SOHO/LASCO images. We also see that while the dynamic pressure prediction is not very good at Earth it is very good at Mars and that the reason for the bad determination of dynamic pressure at Earth is the density prediction rather than the speed prediction, as also found by *Taktakishvili et al.* [2009] and *Falkenberg et al.* [2010].

5.2. Evaluation of Using Flare Location as Initial Direction

[33] Theoretically, if an ICME moves radially from its point of origin on the solar surface, and if the CME is associated with a flare, then the flare location should be a good indication of the direction of the ICME, and could therefore be used as the direction input in ENLILv2.6. *Temmer et al.* [2009] reported that the flare location is a good proxy of the CME source location and therefore also of the CME direction if radial propagation is assumed, based on a study of slower CMEs than those presented here. *Falkenberg et al.* [2011] found for the 17 November 2001 CME (Event 5 in this study) that the CME direction inferred from the flare origin longitude yielded significantly improved simulation results compared to the longitudinal component of the directions found by both the manual and the automated method. Using the flare origin longitude as CME direction in this case allowed the ICME to encounter both Mars and Earth in a manner corresponding to observations, while the simulated ICME largely missed Mars when using the longitudes found by both the manual and the automated method.

[34] Figure 4 shows the longitude and latitude found by the two input parameter methods against the locations of the assumably related flare events (Table 2). The blue dots indicate ICMEs that in the simulations encountered both Mars and Earth, red dots indicate ICMEs that did not encounter Earth, green dots indicate ICMEs that did not encounter Mars, and purple dots indicate ICMEs that did not encounter either planet. ICMEs that did not encounter Earth in the simulations when using the flare origin as direction were primarily limb events (|heliocentric longitude| >80°) and very southernly events (heliocentric latitude ~−20°). The events not encountering Mars were primarily the same as those not encountering Earth, however a couple of additional less systematic events are also evident. The spread in heliocentric longitude is much larger for the flare locations than for the directions found by either input parameter method.

[35] The simulation results obtained using the flare locations from Table 2 and the time, speed and half-angle widths from Table 3 are listed in Table 6 together with the satellite data for both planets, so the data and the two simulations are easily compared for each event. Using the same direction, the simulations done with the manual parameters still consistently arrive earlier than the simulations done with the automatic parameters (with the exception of Event 5) because the speeds found by the manual method are generally higher than those found by the automated method. For Event 14 the speed found by the automated method is slightly higher (1233 km/s) than that found by the manual method (1193 km/s) however the ICME using the manual parameters still arrives first when using the same direction. This could be due to the half-angle widths found by the two methods (41° and 71° respectively) where the simulation using the manual method parameters has a wider ICME.

[36] Several events fail to encounter one or both planets. Events 1 and 11 fail to encounter either planet for both methods. These are both eastern limb events (Table 2) so this is not very surprising as Mars and Earth are separated by 33° and 20° in heliocentric longitude respectively. Event 8 only encounters Earth for the manual method, and does not encounter Mars for either method. This is a W42 flare, but the half-angle width found by the automated method is only 30°, so it is not surprising that the automated method ICME fails to encounter Earth. Mars is trailing Earth by 77° and is therefore not likely to be hit by a western event at all. Events 3 and 7 fail to encounter Earth for both methods, but does encounter Mars. Again these events are limb events at W85 and E90 so it is not surprising that they fail to encounter Earth. Mars at these times is leading Earth slightly (26°) for the western event and trailing Earth by 72° for the eastern event and it is

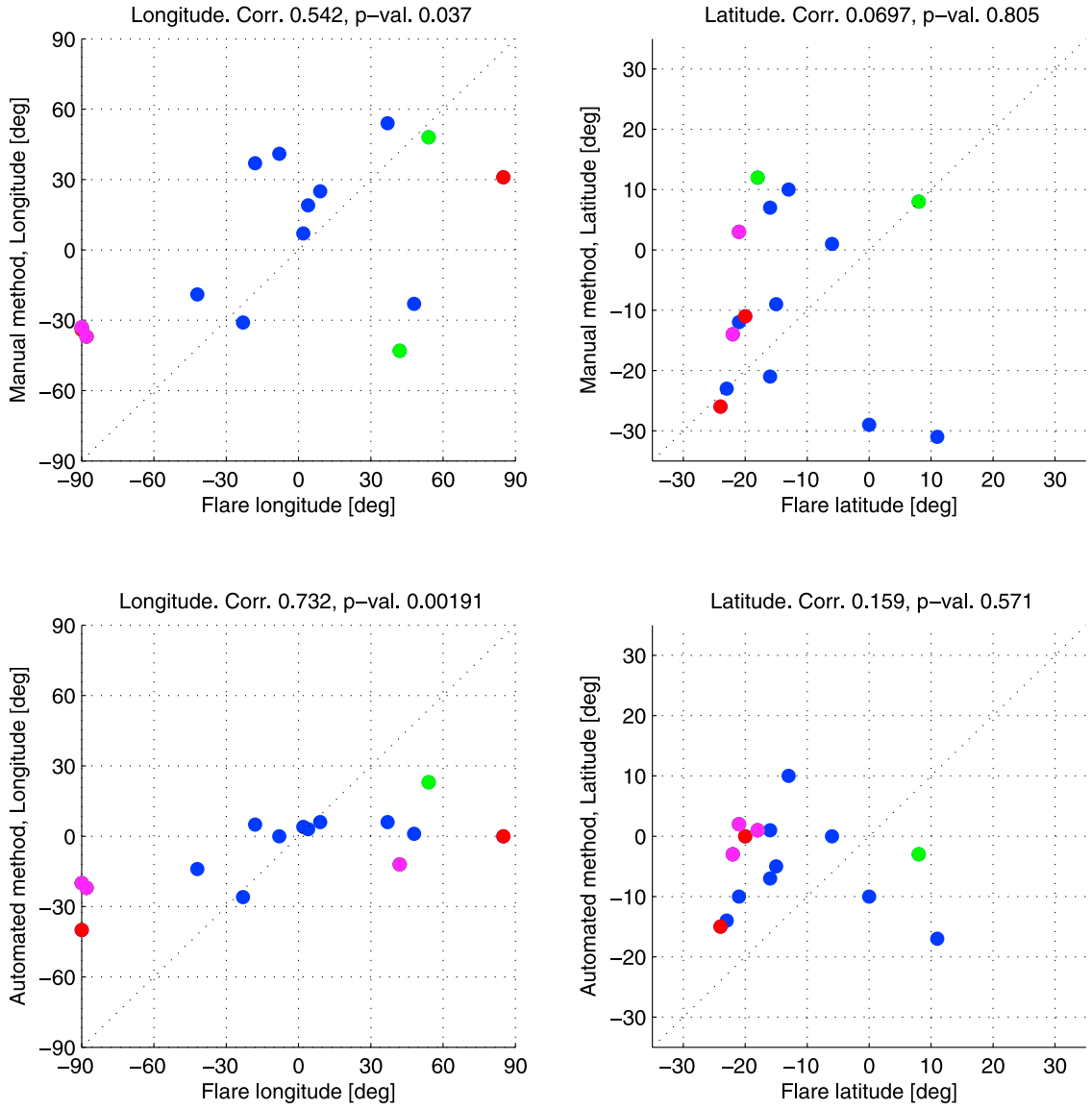

Figure 4. (left) The longitude and (right) latitude found by (top) the manual method and (bottom) the automated method against the flare locations from Table 2. Blue dots indicate ICMEs that encountered both Mars and Earth, red dots did not encounter Earth, green dots did not encounter Mars, and purple dots did not encounter either planet. "Corr" is the correlation coefficient of the points, and "p-val" is the probability of achieving the same correlation coefficient for randomly distributed points.

therefore quite logical that Mars is encountered by the ICME in both of these cases, though only grazed in the case of the western event (Event 3) and therefore arriving much too late Mars (Table 6). Event 6 fails to encounter Mars for both methods which is again not surprising as the flares are western flares (W48 and W54) and Mars is trailing Earth by 71° (Table 2).

[37] The absolute and absolute error in arrival time and dynamic pressure between the simulations and the satellite data is plotted in Figure 5, where we see the same tendencies as we did in Figure 3 though with slightly fewer data points, as several ICMEs failed to encounter one or both planets when using the flare location as direction. Again the second Halloween 2003 CME (Event 13) accounts for the worst for the dynamic pressure predictions at Earth for both methods. The linear tendencies in the dynamic pressure deviations are still present, now with a correlation of 83.4% at Mars and 99.9% at Earth. The average and average absolute of the values from Figure 5 are listed in Table 7. We again see the same

Table 6. Results of the Simulations Using the Flare Locations From Table 2 and the Speed and Half-Angle Width Listed in Table 3[a]

	Mars		Earth			
	Arrival Time (UT)	P_{dyn} (nPa)	Arrival Time (UT)	P_{dyn} (nPa)	Speed (km/s)	Density (cm^3)
Event1 data	2001/04/04 21:40	8	04/04 15:00	9.7	800	11.3
Event1 man						
Event1 auto						
Event2 data	2001/04/12 11:00	10	04/11 13:40	32	760	38.5
Event2 man	2001/04/12 17:16	42.2	04/11 15:21	168	975	105.5
Event2 auto	2001/04/13 09:36	12.3	04/11 22:33	75.2	810	89
Event3 data	2001/04/19 03:35	2.5	04/18 08:35	19.2	535	40
Event3 man	2001/04/21 04:48	3.1				
Event3 auto	2001/04/21 06:00	2.8				
Event4 data	2001/09/25 19:55	14	09/25 20:45	39	650	52
Event4 man	2001/09/26 03:50	49.2	09/25 17:38	140.2	805	129
Event4 auto	2001/09/27 15:21	16	09/27 00:00	26	445	79
Event5 data	2001/11/20 03:35	12	11/19 18:15	7.5	622	20
Event5 man	2001/11/21 06:57	4.8	11/20 04:33	2.7	445	8.2
Event5 auto	2001/11/20 18:28	6.6	11/19 22:33	3.8	461	10.5
Event6 data	2001/12/29 06:30	23.6	12/29 05:25	25	455	80
Event6 man			12/27 09:36	115.3	830	190
Event6 auto			12/30 06:00	14.2	580	52.5
Event7 data	2001/12/31 18:00	7	12/30 20:15	9.1	700	8
Event7 man	2001/12/31 00:00	52				
Event7 auto	2002/01/01 04:48	23				
Event8 data	2002/01/11 06:45	8.8	01/10 16:20	10.7	650	18
Event8 man			01/10 07:40	39.5	940	26.8
Event8 auto						
Event10 data	2003/05/31 03:45	8	05/30 16:20	23.8	800	25
Event10 man	2003/06/01 00:00	17.6	05/31 00:00	44.5	722	51
Event10 auto	2003/06/01 18:28	10.8	05/31 20:02	8.7	585	19
Event11 data	2003/10/25 09:35	17.5	10/24 15:20	36	600	60
Event11 man						
Event11 auto						
Event12 data	2003/10/30 05:30	21.3	10/29 06:10	56.6	2300	18
Event12 man	2003/10/29 22:48	71.8	10/29 10:33	266	1300	104.6
Event12 auto	2003/10/31 07:26	15	10/30 06:14	57	675	74
Event13 data	2003/10/31 11:30	20	10/30 20:00	5.4	1800	1
Event13 man	2003/10/31 21:36	18.4	10/31 08:24	91.2	1150	51.4
Event13 auto	2003/11/01 08:24	4.4	10/31 12:00	31	957	25.5
Event14 data	2003/11/21 04:50	4.5	11/20 08:25	19.6	750	28
Event14 man	2003/11/21 11:24	12.4	11/20 05:39	32.8	815	32.3
Event14 auto	2003/11/21 21:36	8.4	11/20 09:50	16	684	22.7

[a]Listed for each event simulated is the satellite data and the results using the manual method and the automated method. The parameters listed are the arrival time at both Mars and Earth as well as the maximum dynamic pressure seen during the ICME arrival, and for Earth the maximum speed and density are also given. When no data is listed the simulated ICME did not encounter the planet.

tendencies as described in section 5.1, however, still based on fewer data points, allowing Event 13 to influence the statistics even more.

[38] Overall, no improvement is seen by applying the flare location as the direction and using the time, speed and half-angle widths found by the two input parameter methods, especially not when considering the importance of an ICME shock front in fact encountering a planet, when it was known to do so through satellite data. This may be due to at least four things.

[39] First, the remaining input parameters should be recalculated for both input parameter methods, assuming the direction is now given by the flare location, as the conic parameters are coupled. This would, for example mean that limb events must be assumed to be wider than 90° in order to appear as halo events in the SOHO/LASCO images. This is currently not allowed by either input parameter method, but is allowed in ENLILv2.6. It would also affect the radial speeds found by both methods, and perhaps the start times.

[40] Second, recent STEREO based studies [*Kilpua et al.*, 2009; *Liu et al.*, 2010; *Pomoell et al.*, 2010; *Byrne et al.*, 2010] have indicated that ICMEs are deflected latitudinally toward the Sun's equator, implying that while the heliocentric longitude of the flares may indicate the ICME direction, the heliocentric latitude of the flare should largely be ignored and a heliocentric latitude close to the equator should be used. These studies are, however, mainly based on slow, less massive CMEs due to the operation period of STEREO and the lack of fast and massive CME events in recent years. The possible deflection of the CMEs is somewhat corrected for by using

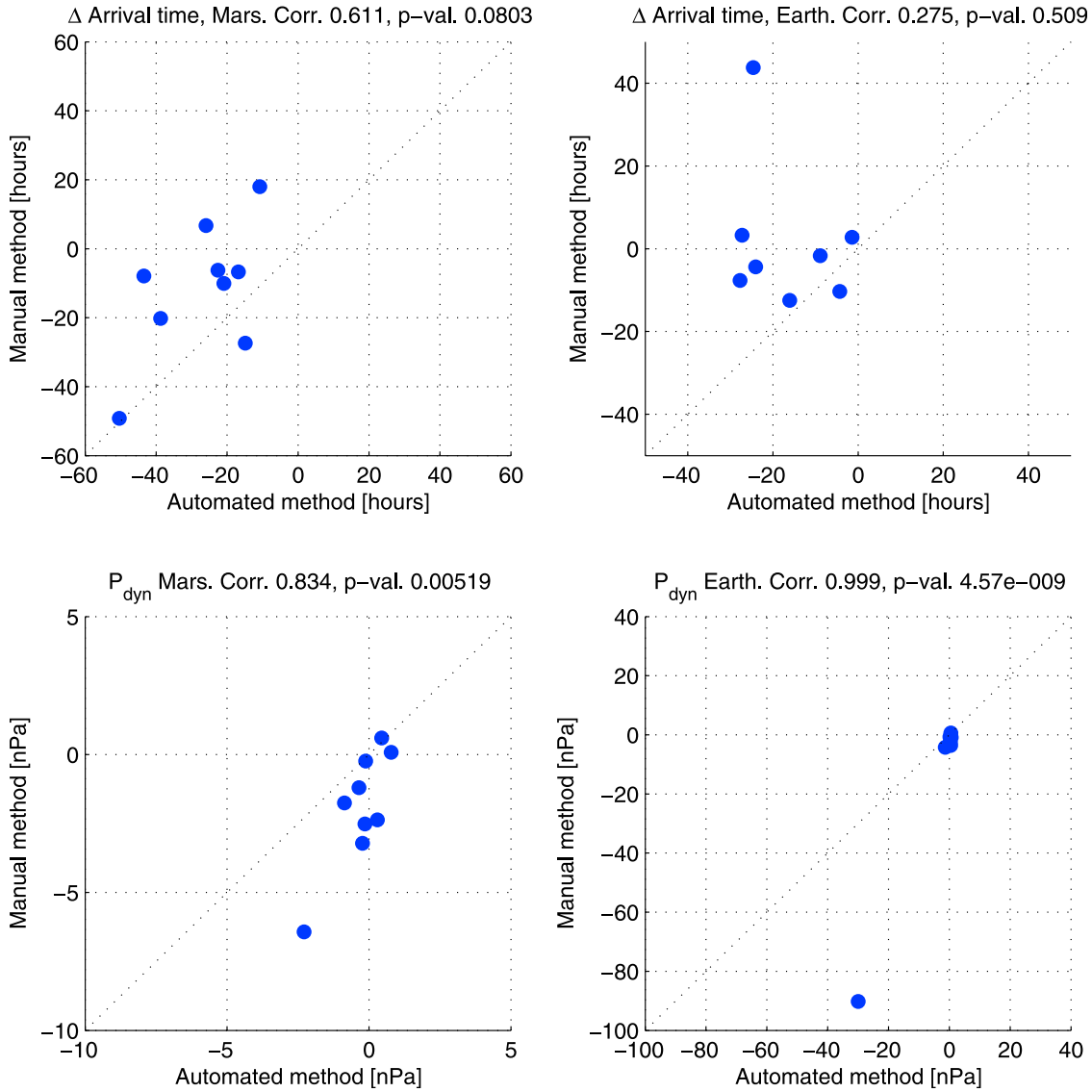

Figure 5. The deviation (top) in arrival time and (bottom) in the maximum P_{dyn} reached during the ICME arrival for (left) Mars and (right) Earth using the flare locations from Table 2 and the speed and half-angle width listed in Table 3. Δ arrival time is calculated as data minus model, ergo negative values indicate that the event arrived later in the simulation than in the satellite data. The deviation in P_{dyn} is calculated as data minus model divided by data, ergo a value of –5 means the dynamic pressure was overestimated by 5 times in the simulation in relation to the satellite data. "Corr" is the correlation coefficient of the points, and "p-val" is the probability of achieving the same correlation coefficient for randomly distributed points.

the SOHO/LASCO C3 images which have a larger field of view (~37 R_S).

[41] Third, perhaps the CMEs do not propagate radially, or are deflected significantly in the inner heliosphere (i.e., below the inner boundary of ENLILv2.6 of 21.5 R_S), so that the flare location is therefore not a good indication of the ICME direction. Again this is somewhat corrected for by using the larger field of view SOHO/LASCO C3 images.

[42] Fourth, possible ICME structure is not taken into account in ENLILv2.6, e.g., the density may not be evenly distributed in the ICME shockfront, and the magnetic cloud is not included in the simulations.

[43] One should also be aware that the CME/flare relation for Events 6a and 8a is a little uncertain as these flares were not found to be related to the CMEs by *Gopalswamy et al.* [2007].

Table 7. Average and Average Absolute of the Values Plotted in Figure 5 as Well as Average and Average Absolute Error of the Density and Speed at Earth[a]

		Average Error		Average Absolute Error	
	Type	Mars	Earth	Mars	Earth
Arrival time (h)	Manual	−11.448	1.953	16.941	10.071
	Automated	−27.155	−16.793	27.155	16.793
P_{dyn}	Manual	−1.894	−11.866	2.045	12.009
	Automated	−0.274	−3.629	0.613	4.208
Speed	Manual		−0.078		0.340
	Automated		0.221		0.306
Density	Manual		−6.767		6.898
	Automated		−3.524		3.836

[a]Results of using the flare locations from Table 2 and the speed and half-angle width listed in Table 3. P_{dyn}, speed, and density are determined by data minus model divided by data.

5.3. Using SOHO/LASCO Catalogue Speed at 20 R_s

[44] The speeds found by the two input methods are often lower than those listed in the SOHO/LASCO catalogue at 20 R_S [*Gopalswamy et al.*, 2009; *Yashiro et al.*, 2004] (Figure 6) especially for the automated method. The SOHO/LASCO catalogue speed is based on height-time measurements of SOHO/LASCO images and is therefore the plane-of-sky speed. Geometrically the radial speed will always be higher, or at least equal to, the plane-of-sky speed when assuming a cone-like propagation [*Michałek et al.*, 2003]. The effect is larger for events marked as fast in the SOHO/LASCO catalogue (Figure 6).

[45] The SOHO/LASCO speeds are found as pure height-time measurements of the leading edge of the CME, i.e., they measure the height of the fastest moving part of the CME in the SOHO/LASCO C2 and C3 images [*Gopalswamy et al.*, 2009; *Yashiro et al.*, 2004]. The two input parameter methods, respectively, draw ellipses around the outline and fit a cone to them, and digitally determines the CME area and fits a cone-like feature to this. Fitting a cone to the CME area in the SOHO/LASCO images means that outliers are less influential on the results, and a small fast moving parts, on which the SOHO/LASCO speed is based, may not be attributing much to the results of the automated method. Drawing ellipses around the outline means that you are more likely to include smaller fast moving features and these are contributing significantly to the results, if included. The manual method therefore corresponds better to the method used to find SOHO/LASCO 20 R_S speeds. *Michałek et al.* [2003] reported that using their input parameter method, the radial speed on average was 20% higher than the SOHO/LASCO plane-of-sky speed. *Reiner et al.* [2003] reported, based on in situ observations of two halo CMEs, the radial speed to be 1.4 times higher than the SOHO/LASCO plane-of-sky speed. The speeds found by the manual method are on average 9% lower and the speeds found by the automated method are 26% lower than the 20 R_S speed from the SOHO/LASCO catalogue, for the events treated here. One must attribute this discrepancy to the fact that the two input parameters do not find the plane-of-sky speed, however it seems that both input parameter methods underestimate the speed of CMEs. For the manual method, some speeds seem to be vastly overestimated (Figure 6), while others are vastly underestimated. For the automated method, speeds of events with SOHO/LASCO 20 R_S speeds of ≤1500 km/s correspond well within the uncertainty of the automated method, however for faster events, the automated method seems to underestimate the speed significantly.

[46] We tried to estimate, for each simulation in Table 4, whether changing the speed toward the SOHO/LASCO catalogue 20 R_S speed (i.e., make the event faster or slower) would in fact improve the arrival time in the simulation at either planet. The results are shown in Tables 8 and 9 for the manual and automated method, respectively. For the automated method, we see that the arrival time at both planets would generally be improved by changing the initial speed in the direction of the SOHO/LASCO 20 R_S speed (i.e., increasing or decreasing the speed), which for all events, except Event 3a, means increasing the speed. Event 3a is also the only event not improved at Mars for the automated method. This reflects, as Table 5 showed, that when applying the automated method, the ICME always arrived late at Mars, and generally late at Earth. For the manual method the arrival time would be improved in general for Mars by changing the initial speed in the direction of the SOHO/LASCO 20 R_S speed, while at Earth, five events would be improved while seven would not. For the manual method changing the speed toward the SOHO/LASCO 20 R_S speed does not always mean increasing the speed and the results are therefore more varied, also the simulations with the manual method parameters in general arrive late at Mars and early at Earth and it is therefore expected that changing the speed in either direction can not generally improve the arrival time at both planets. In summary, the speeds found by the automated method seem to be underestimated, while the speeds found from the manual method are too variable to be improved on easily.

5.4. CME Width

[47] As discussed in section 5.3, the SOHO/LASCO catalogue speeds are all plane-of-sky speed and should therefore, theoretically be lower than the true radial CME speeds. From the results presented in sections 5.1 and 5.2, it seems that assuming a speed ~20% higher than the SOHO/LASCO R_S speed, would yield simulations arriving much too early at Earth. Assuming that the SOHO/LASCO R_S speed is the actual CME speed entails assuming that the expansion speed ≃ the radial speed, i.e. the event must be very wide. *Pulkkinen et al.* [2010] use a climatological value of 30° for the half-width of the ICMEs based on the statistics presented by *St. Cyr et al.* [2000] and *Yashiro et al.* [2004]. Both of these statistics where based on nonhalo CMEs exclusively, and *Yashiro et al.* [2004] even notes that halo CMEs are expected to be much faster and much wider

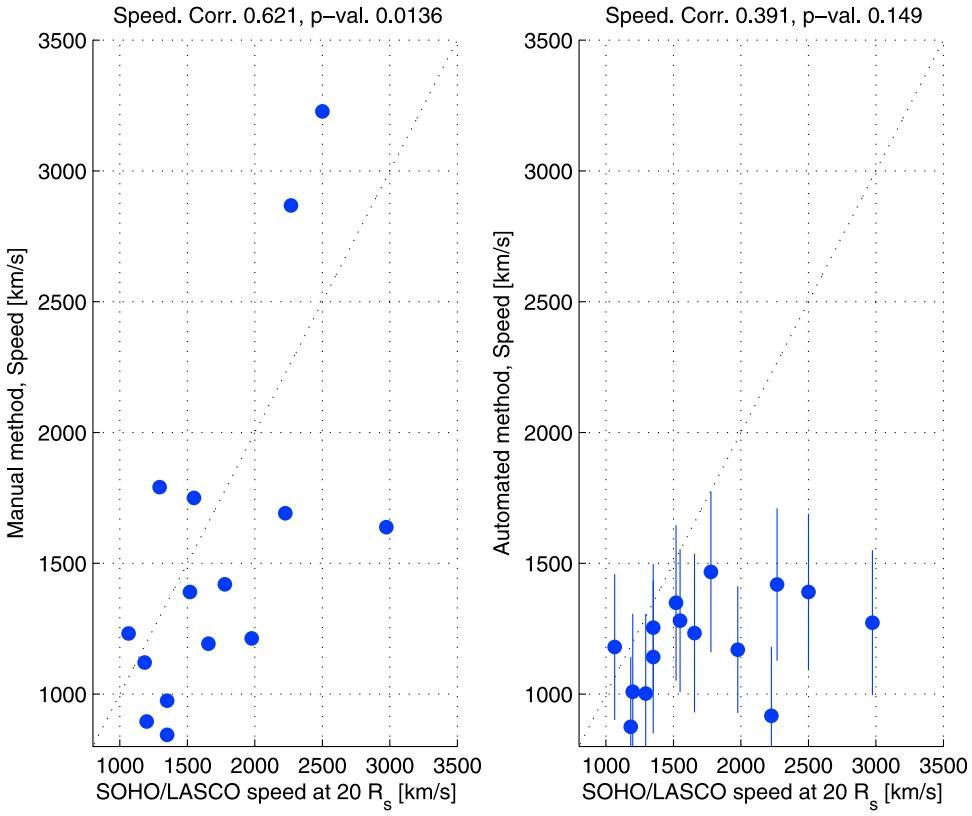

Figure 6. Comparison of the speed found by (left) the manual method and (right) the automated method to the SOHO/LASCO catalogue speed at 20 R_S. "Corr" is the correlation coefficient of the points, and "p-val" is the probability of achieving the same correlation coefficient for randomly distributed points.

than nonhalo CMEs, a finding supported by *Michałek et al.* [2003] who finds the average half-angle width of halo CMEs to be 60°. The climatological value in the automated method is, however, only used to stabilize solutions (e.g., for events originating close to W00N00), and running the automated method with a climatological value of 60° had almost no impact on the input parameters. As both input parameter methods are only valid for halo CMEs, the larger widths found from by the manual method seem more realistic. This is confirmed by the fact that more shock events fail to encounter both planets, as expected from the data, for the simulations done with the automated method parameters compared to simulations done with the manual method parameters.

5.5. Background Features

[48] Event 6 is an interesting case because the shock arrived almost simultaneously at Earth and Mars (Table 1). In the only simulation which encounters both planets for this event, the simulation done using the parameters from the manual method listed in Table 3, the event also encounters Earth and Mars almost simultaneously, although almost 2 days too early (red line in Figure 7). The feature present in the simulations at Mars data prior to the shock arrival is also present in the simulation using the automated method parameters, even though that ICME does not encounter Mars. From the actual propagation of the ICMEs (Figure 8) it is clear that this feature is a high speed stream present in the background solar wind. It is this feature that enables the simulation done with the manual method parameters to arrive almost simultaneously at the two planets, because the part of the ICME shock front that interacts with the high speed stream propagates faster. Figure 8 also shows us that while Event 6a does encounter Mars in the simulation with the manual method parameters, Event 6b does not. In both simulations, Events 6a and 6b are virtually merged and arrive almost simultaneously at Earth, however, there is clear evidence in the simulations of two ICMEs arriving. We also see clearly why the ICMEs specified by the automated method parameters could never encounter both Earth and Mars due to their width. Event 4 also encounters Mars and Earth almost simultaneously (Table 1), in fact it seems to arrive at Mars approximately a half an hour earlier. Again a high-speed stream is present in the simulation, however for this event the effect of the high-speed stream in the simulations is not enough for the simulations to replicate the simultaneous arrival at the two planets.

Table 8. Estimation of Whether Changing the Speed Found by the Manual Method Toward the SOHO/LASCO Catalogue Speed at 20 R_S Would Improve the Arrival Time at Either Mars or Earth[a]

	Δ Arrival Time, Mars (h)	Δ Arrival Time, Earth (h)	Input Speed (km/s)	SOHO/LASCO Speed at 20 R_s (km/s)	Improve at Mars	Improve at Earth
Event1a		27	1750	1549		y
Event2a			895	1198		
Event2b	−1.44	−0.48	1638	2974	n	n
Event3a	−1.2	12.648	1232	1064	n	y
Event4a	−7.92	1.08	3227	2500	n	n
Event5a	−42.72	3.84	844	1350	y	n
Event6a			1420	1778		
Event6b	36.96	46.188	1791	1295	y	y
Event7a	13.92	16.68	1691	2226	n	n
Event8a	−13.44	2.4	1213	1977	y	n
Event10a	−21.192	−13.44	1121	1184	s	s
Event11a	−31.2	−27.84	975	1350	y	y
Event12a	3.12	−5.328	2868	2268	y	n
Event13a	−11.28	−15.12	1390	1519	y	y
Event14a	−45.6	−0.24	1193	1656	y	n
Total improved					7y 4n	5y 7n

[a]Y denotes yes, n denotes no, and s denotes same. If no answer is listed the ICME in the simulation did not encounter the planet or the event in question is a merged shock, that is, two CMEs are attributed to the same shock front and therefore only one Δ arrival time is available. If Δ arrival time in the original simulation was less than 1.5 h, we estimate that the results would not be improved by changing the initial CME speed in the simulation. The total improved row sums up the number of yes and no answers in the rows above for each planet.

[49] Event 4 and 6 are very good examples of the importance of the background features in the solar wind to ICME propagation. Features like high speed streams or current sheet crossings can dramatically affect both the shape and the propagation of a simulated ICME, it is therefore important to consider these phenomena when trying to produce a best-fit simulation. ENLILv2.6 does allow the user to interfere with the background solar wind conditions, though this option is not directly available through the CCMC interface. Another factor is the background solar wind input to ENLILv2.6, in this study the WSAv1.6 model using MWO magnetograms (or in the case of Events 3, 6 and 7, the MAS model). Here both the quality of the magnetogram in question is an issue, but also the performance of the model. We leave this subject to future efforts.

5.6. Between Earth and Mars

[50] The results presented in section 5.1 show that for the manual method, shock arrival is usually early at Earth

Table 9. Estimation of Whether Changing the Speed Found by the Automated Method Toward the SOHO/LASCO Catalogue Speed at 20 R_S Would Improve the Arrival Time at Either Mars or Earth[a]

	Δ Arrival Time, Mars (h)	Δ Arrival Time, Earth (h)	Input Speed (km/s)	SOHO/LASCO Speed at 20 R_s (km/s)	Improve at Mars	Improve at Earth
Event1a		6.60	1281	1549		n
Event2a			1009	1198		
Event2b	−15.36	−6.48	1273	2974	y	y
Event3a	−6.00	14.33	1180	1064	n	y
Event4a	−41.28	−27.24	1390	2500	y	y
Event5a	−37.20	12.48	1142	1350	y	n
Event6a			1467	1778		
Event6b		41.39	1002	1295		n
Event7a	−12.00	−0.12	917	2226	y	n
Event8a		3.60	1170	1977		n
Event10a	−39.91	−14.88	875	1184	y	y
Event11a	−27.60	−26.64	1254	1350	y	y
Event12a	−22.08	−23.09	1419	2268	y	y
Event13a	−19.68	−15.36	1349	1519	y	y
Event14a	−36.00	−0.72	1233	1656	y	n
Total improved					9y 1n	7y 6n

[a]Y denotes yes and n denotes no. If no answer is listed the ICME in the simulation did not encounter the planet or the event in question is a merged shock, that is, two CMEs are attributed to the same shock front and therefore only one Δ arrival time is available. If Δ arrival time in the original simulation was less than 1.5 h, we estimate that the results would not be improved by changing the initial CME speed in the simulation. The total improved row sums up the number of yes and no answers in the rows above for each planet.

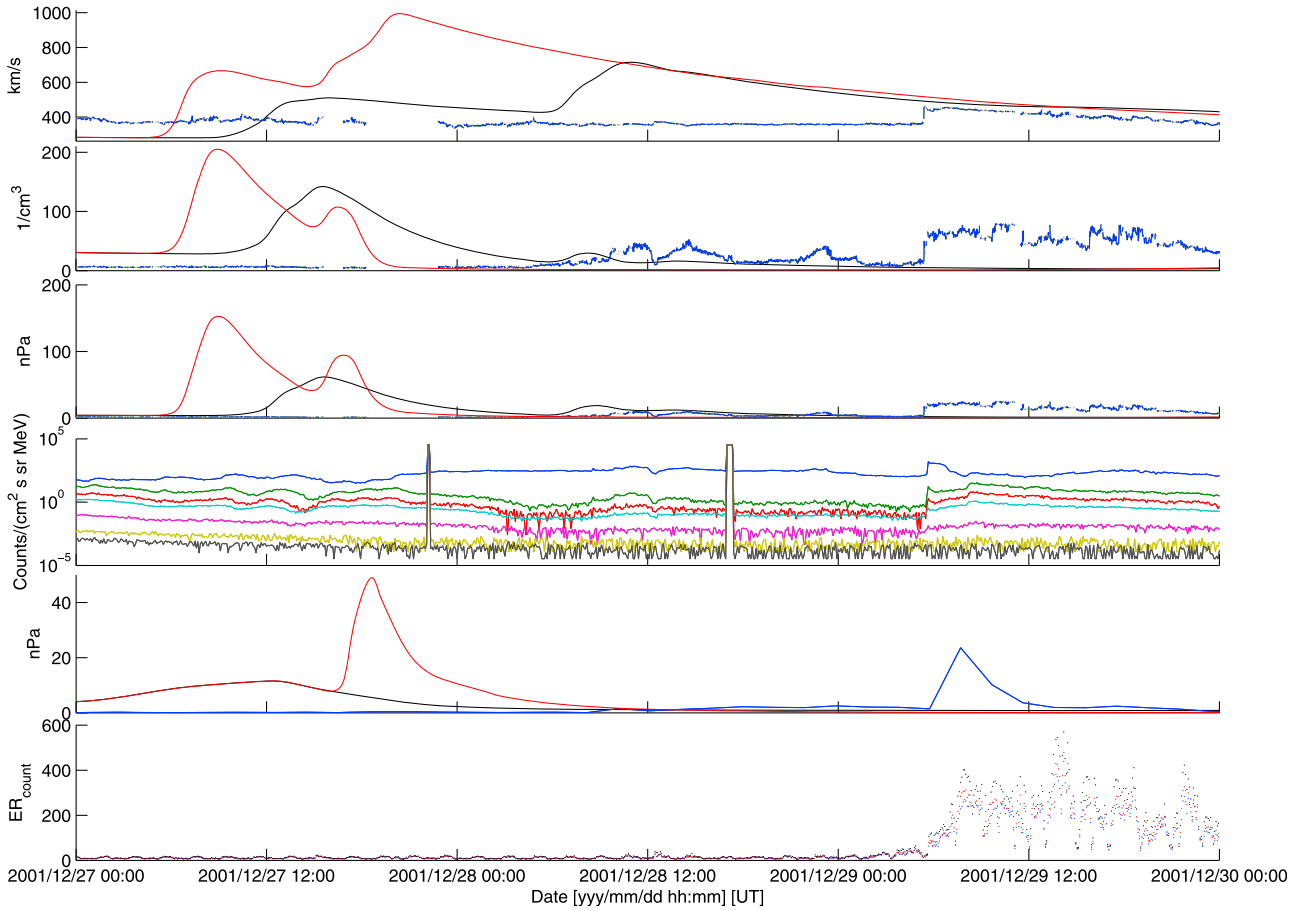

Figure 7. Data and simulations for Event 6. From top to bottom, the panels show OMNI data from near Earth (top two panels), the dynamic pressure calculated from the OMNI data, GOES data, the pressure proxy at Mars calculated from MGS magnetic field measurements, and the background count rate from the MGS ER instrument. The red line shows the simulation done with the manual method parameters from Table 3, and the black line shows the simulation done with the automated method parameters from Table 3. The GOES energy channels are (from top to bottom) 0.8–4 MeV, 4–9 MeV, 9–15 MeV, 15–40 MeV, 40–80 MeV, 80–165 MeV, and 165–500 MeV. Spurious data points are seen in the highest energy channels; these should be ignored.

and late at Mars. For the automated method the shock arrival is usually late at both planets, however much more so at Mars than Earth. This indicates that generally the travel time between Earth and Mars is overestimated in ENLILv2.6 using either input parameter method. As a first order approximation one would assume that the time lapse between shock arrival at the two planets should be approximately equal to the radial distance divided by the speed measured at Earth, and the radial distance between Earth and Mars is approximately 0.5 AU varying slightly through the orbit of both planets. The average radial distance between Mars and Earth for the events studied here is 0.46 AU. If we use the predicted arrival times by ENLILv2.6 with either input parameter method and the predicted speed at Earth (Figure 9, top) it seems that the time lapse between shock arrival at Earth and Mars is approximately equal to radial distance divided by speed at Earth in the ENLILv2.6 simulations. Deviations reflect the fact that ICME shocks are curved and encounter the two planets differently depending ICME width and direction as well as the location of the planets. Comparing the time lapse between the predicted shock arrival at Earth and Mars to the measured time lapse (Figure 9, bottom), it does in fact take too long between the shock arrival at Earth and Mars in the simulations compared to what was measured. If we compare the measured time lapse between shock arrival at Earth and Mars to the radial distance divided by speed measured at Earth (Figure 10), we see that the ICME shocks do in fact have a shorter time lapse between shock arrival at Earth and Mars than what would be expected from the speeds measured at Earth. Again one must consider that a shock front is a curved structure of a certain width where, perhaps, one part travels faster than the rest (see, e.g., section 5.5), but it is notable that the

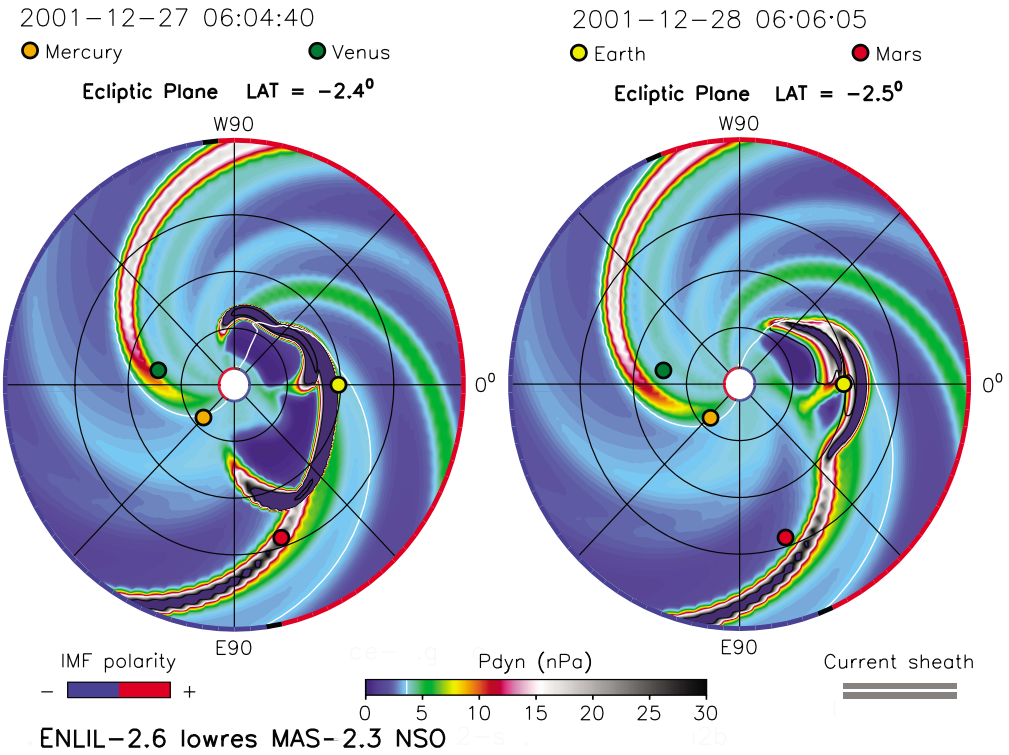

Figure 8. Snapshots of simulations for Events 6a and 6b done with (left) the manual method parameters from Table 3 and (right) the automated method parameters from Table 3. Plot shows dynamic pressure in the ecliptic plane. Note that the dates for the two images are different, the one for the automated method parameters (Figure 8, right) being a day later than the one for the manual method parameters (Figure 8, left).

actual travel time from Earth to Mars is so much lower than radial distance divided by speed measured at Earth in all but 2 of the events studied here. The average distance the ICMEs would have traveled in the time it took between the shock arrival at Mars and the shock arrival at Earth, based on their speeds measured at Earth, is 0.37 AU, i.e., 81% of 0.46 AU, for the events presented here (this is not counting Event 4 where the shock arrived at Mars before it arrived at Earth). This could perhaps be because the ICME is still expanding at this point, which has earlier been proposed from multipoint studies of ICMEs [*Farrugia et al.*, 1995; *Jian et al.*, 2008]. A large part of this effect could also be attributed the curvature of ICME shock fronts if one assumes that the majority of the events studied here were in fact directed toward Mars. Assuming that the majority of the events studied here were directed toward Mars may be a plausible assumption considering that only 16 shocks were identified in the periods of 2001 and 2003 when Earth and Mars were separated by less than 80° in heliocentric longitude. This would indicate that our criteria for shock detection at Mars only finds very strong shocks caused by fast and massive ICMEs hitting Mars more or less full on.

[51] It is also notable that the dynamic pressure prediction at Mars corresponds so much better to observations than at Earth (section 5.1). From Figure 1, the dynamic pressure proxy measured at Mars is approximately $1/r^2$ of the dynamic pressure measured at Earth. We use the average radial distance to Mars for the events studied here, i.e. 1.45 AU. If we make a similar plot of the predictions of dynamic pressure made by ENLILv2.6 with the two input parameter methods (Figure 11) we see that the pressure in ENLILv2.6 at Mars does in fact fall off faster than $1/r^2$. Again one should remember that the direction and width of the ICME plays a large role here, as well as the location of the two planets, however, one would still expect the results to resemble those in Figure 1.

6. Conclusions

[52] We have performed at study of ICME propagation and prediction capabilities. We have tested the results of running ENLILv2.6 with CME input parameters from both the manual method presented by *Xie et al.* [2004] and the automated method presented by *Pulkkinen et al.* [2010] for 15 ICMEs, based on shock events identified at Mars using MGS data in periods in 2001 and 2003 when Earth and Mars were separated by less than 80°. We find the following.

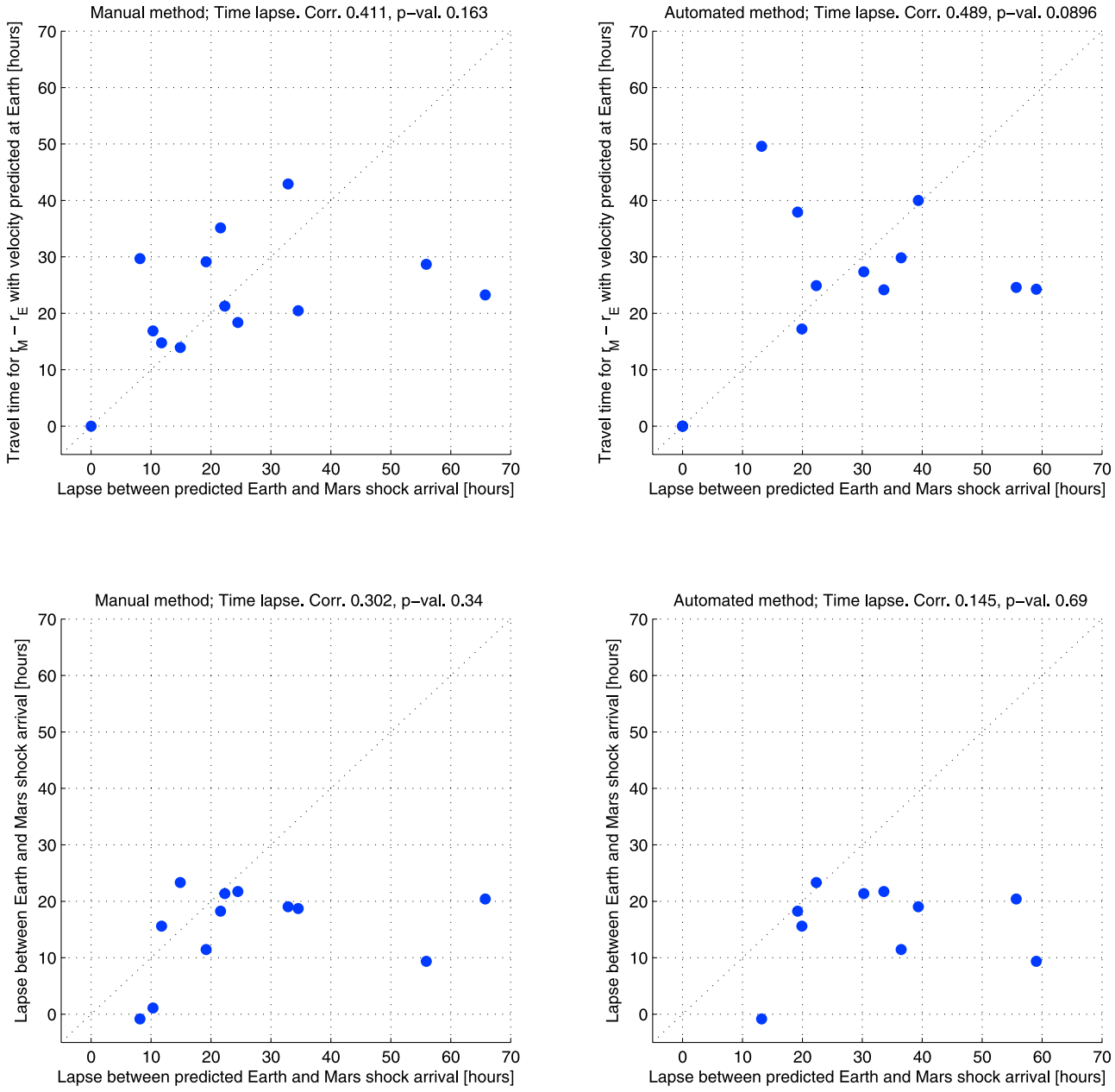

Figure 9. Time lapse between shock arrival at Earth and Mars in ENLILv2.6 using (left) manual method input parameters and (right) automated method input parameters against (top) radial distance divided by speed predicted at Earth and (bottom) the measured time lapse between shock arrival at Earth and Mars using OMNI and MGS data, respectively. Values used are listed in Table 4. "Corr" is the correlation coefficient of the points, and "p-val" is the probability of achieving the same correlation coefficient for randomly distributed points.

[53] 1. The results obtained from ENLILv2.6 simulations using input parameters found by the manual method and the automated method do not differ greatly. However, in 3 of 13 simulations the simulations with the automated parameters fails to encounter both planets due to a smaller ICME width. Simulations with the manual parameters only fails to encounter both planets in one simulation. The arrival time prediction for both methods is similar, though slightly better for the manual method, with an average absolute error of about 13.3 h and 14.8 h at Earth, and 19 h and 28 h at Mars, for the manual and automated methods respectively. The difference in arrival time prediction at Mars is not statistically significant. Both methods generally predict ICME shocks that arrive too late at Mars.

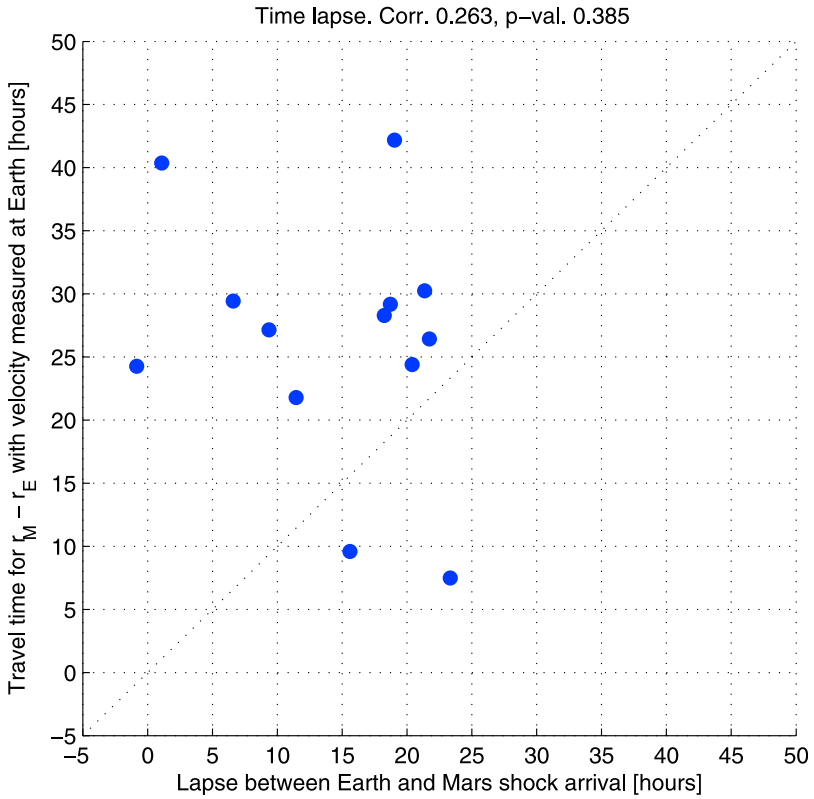

Figure 10. Time lapse between shock arrival at Earth and Mars using OMNI and MGS data, respectively, against radial distance divided by speed measured at Earth. Values used are listed in Table 1. "Corr" is the correlation coefficient of the points, and "p-val" is the probability of achieving the same correlation coefficient for randomly distributed points.

The manual method statistically predicts too early ICME arrival at Earth whereas the automated method predicts too late arrival. The dynamic pressure found by the automated method is generally lower at both Earth and Mars, and is better predicted by ENLILv2.6 when using the parameters from the automated method. We also find that in general both the width and the speed are underestimated by the automated method, and that the speed found by the manual method compared to the SOHO/LASCO plane-of-sky speed, varies in a nonsystematic way compared to the errors in arrival time observed here.

[54] 2. Using the flare location as direction of the ICME and leaving the remaining parameters found by the two input parameter methods intact, does generally not improve the results. Not only did several ICMEs fail to encounter Mars or Earth or both, for both input parameter methods, but the ones that did encounter the planets did not result in a statistical improvement of the results. This may be due to the fact that the direction of propagation should be taken into consideration before determining the remaining input parameters in order to truly avoid projection effects. This will be a subject for further studies. Also, limb events which are known to encounter Earth, must either be assumed to be very wide, or to have changed direction relative to their site of origin.

[55] 3. Changing the radial speed estimated by the two input parameter methods toward the SOHO/LASCO catalogue plane-of-sky speed at 20 R_S, would seem to be able to improve the simulation arrival time results. This is true for the automated method at both planets and for the manual method at Mars. For the manual method at Earth, changing the speed would theoretically have improved about half of the simulations.

[56] 4. The 14 shock events identified at Mars, in which we could identify the source of the shock, were caused by fast halo or partial halo events, with the exception of Events 10b and 10c which were still wide and fast events. We also see that all of the 16 shock events identified at Mars in these periods could be associated with a shock event at Earth. The short time lapse between shock arrival at Earth and Mars for these events and the number of shocks identified, indicate that we only identify very strong shocks at Mars, and the majority of the events were directed toward Mars.

[57] 5. Background features in the solar wind, in combination with the imposed ICME/planet configuration, have a large influence on ICME propagation, i.e., the presence of high-speed streams can enable an ICME to arrive simultaneously at Earth and Mars.

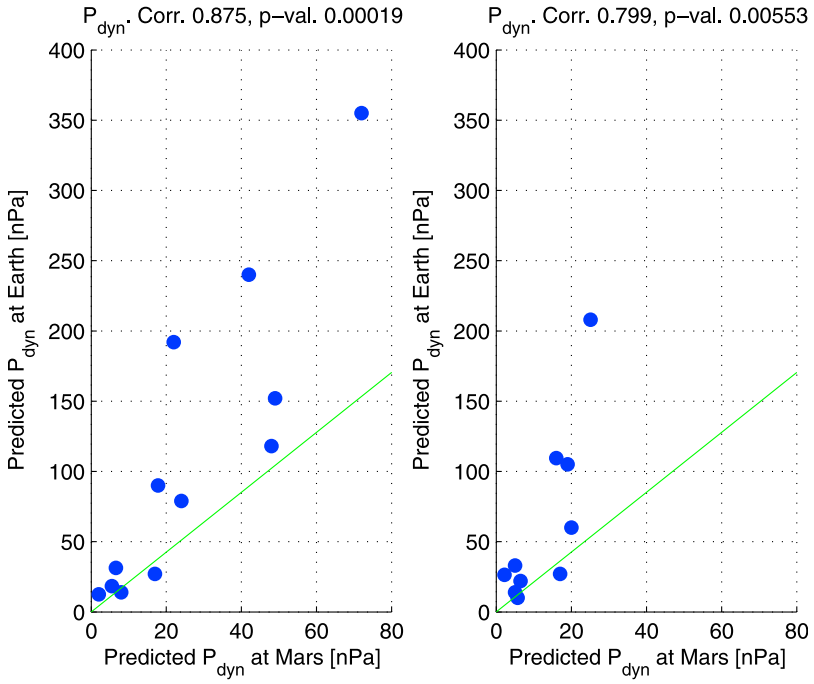

Figure 11. The maximum dynamic pressure predicted by measured by ENLILv2.6 at Earth against that predicted at Mars using (left) manual method input parameters and (right) automated method input parameters. Green line indicates $1/r^2$ propagation of the dynamic pressure at Earth to Mars as found by *Vennerstrom et al.* [2003] and *Crider et al.* [2003] for times of quiet solar wind. Values are listed in Table 4. "Corr" is the correlation coefficient of the points, and "p-val" is the probability of achieving the same correlation coefficient for randomly distributed points.

[58] 6. The time lapse between the shock arrival at Earth and Mars in situ data is less than what was expected from simulations. This may be because the events studied here are primarily events directed toward Mars, or the ICMEs are in fact accelerated between Earth and Mars.

[59] This work will be applied to improve the methods for finding initial transient (CME) parameters used by WSA/ENLIL. Due to the significant role that ICMEs play in driving space weather, improving the methods for finding accurate CME input parameters has major implication from space weather modeling and forecasting viewpoints. For example, understanding ICME and SEP arrival at Mars will be crucial for future Mars-bound manned and robotic missions. Further, being able to model ICME propagation accurately may also help to better understand observational data anomalies experienced by both Mars and interplanetary space science missions.

[60] **Acknowledgments.** All simulations carried out for this work were graciously performed at the Community Coordinated Modeling Center at the NASA Goddard Space Flight Center, whose efforts have been invaluable; special thanks goes to Anna Chulaki, Larisa Moiseev, and Peter Macneice. The OMNI database is generously provided and maintained by Goddard Space Flight Center's National Space Science Data Center, thanks to the cooperation and assistance of the many contributing NASA mission investigators. The SOHO/LASCO CME catalog is generated and maintained at the CDAW Data Center by NASA and The Catholic University of America in cooperation with the Naval Research Laboratory. SOHO is a project of international cooperation between ESA and NASA. The GOES X-ray catalogue and the GOES data is generated and maintained by the National Geophysical Data Center (NGDC), located in Boulder, Colorado, part of the U.S. Department of Commerce (USDOC); the National Oceanic and Atmospheric Administration (NOAA); and the National Environmental Satellite, Data and Information Service (NESDIS), one of three NOAA National Data Centers. The research leading to the results presented in this paper has received funding from European Community's Seventh Framework Programme (FP7/2007-2013) under grant agreement 218816. This study was partially funded by the ESA PRODEX Experiment Arrangement 90322.

References

Arge, C., and V. Pizzo (2000), Improvement in the prediction of solar wind conditions using near-real time solar magnetic field updates, *J. Geophys. Res.*, *105*, 10,465–10,479, doi:10.1029/1999JA000262.

Brain, D. A., J. S. Halekas, R. Lillis, D. L. Mitchell, R. P. Lin, and D. H. Crider (2005), Variability of the altitude of the Martian sheath, *Geophys. Res. Lett.*, *32*, L18203, doi:10.1029/2005GL023126.

Brain, D. A. (2006), Mars Global Surveyor measurements of the Martian solar wind interaction, *Space Sci. Rev.*, *126*, 77–112, doi:10.1007/s11214-006-9122-x.

Brain, D. A., G. T. Delory, R. J. Lillis, D. Ulusen, D. Mitchell, and J. Luhmann (2011), MGS measurements of solar storms and their effects, in *Green Energy from Space Systems: The First International Assessment of the Concept of Space Solar Power*, Int. Acad. of Astronaut., Paris, in press.

Brueckner, G. E., et al. (1995), The Large Angle Spectroscopic Coronagraph (LASCO), *Sol. Phys.*, *162*, doi:10.1007/BF00733434.

Burkepile, J. T., A. J. Hundhausen, A. L. Stanger, O. C. St. Cyr, and J. A. Seiden (2004), Role of projection effects on solar coronal mass ejection properties: 1. A study of CMEs associated with limb activity, *J. Geophys. Res.*, *109*, A03103, doi:10.1029/2003JA010149.

Byrne, J. P., S. A. Maloney, R. T. J. McAteer, J. M. Refojo, and P. T. Gallagher (2010), Propagation of an Earth-directed coronal mass ejection in three dimensions, *Nat. Commun.*, *1*, 74, doi:10.1038/ncomms1077.

Cremades, H., V. Bothmer, and D. Tripathi (2006), Properties of structured coronal mass ejections in solar cycle 23, *Adv. Space Res.*, *38*(3), 461–465, doi:10.1016/j.asr.2005.01.095.

Crider, D. H., D. Vignes, A. M. Krymskii, T. K. Breus, N. F. Ness, D. L. Mitchell, J. A. Slavin, and M. H. Acuña (2003), A proxy for determining solar wind dynamic pressure at Mars using Mars Global Surveyor data, *J. Geophys. Res.*, *108*(A12), 1461, doi:10.1029/2003JA009875.

Dubinin, E., et al. (2008), Structure and dynamics of the solar wind/ionosphere interface on Mars: MEX-ASPERA-3 and MEX-MARSIS observations, *Geophys. Res. Lett.*, *35*, L11103, doi:10.1029/2008GL033730.

Falkenberg, T. V., B. Vršnak, A. Taktakishvili, D. Odstrcil, P. MacNeice, and M. Hesse (2010), Investigations of the sensitivity of a coronal mass ejection model (ENLIL) to solar input parameters, *Space Weather*, *8*, S06004, doi:10.1029/2009SW000555.

Falkenberg, T. V., S. Vennerstrom, D. A. Brain, G. Delory, and A. Taktakishvili (2011), Multipoint observations of coronal mass ejection and solar energetic particle events on Mars and Earth during November 2001, *J. Geophys. Res.*, *116*, A06104, doi:10.1029/2010JA016279.

Farrugia, C. J., V. A. Osherovich, and L. F. Burlaga (1995), Magnetic flux rope versus the spheromak as models for interplanetary magnetic clouds, *J. Geophys. Res.*, *100*, 12,293–12,306, doi:10.1029/95JA00272.

Filippov, B. P., N. Gopalswamy, and A. V. Lozhechkin (2001), Nonradial motion of eruptive filaments, *Sol. Phys.*, *203*, 119–130, doi:10.1023/A:1012754329767.

González-Esparza, J. A., A. Lara, E. Perez-Tijerina, A. Santillan, and N. Gopalswamy (2003), A numerical study on the acceleration and transit time of coronal mass ejections in the interplanetary medium, *J. Geophys. Res.*, *108*(A1), 1039, doi:10.1029/2001JA009186.

Gopalswamy, N., A. Lara, R. P. Lepping, M. L. Kaiser, D. Berdichevsky, and O. C. St. Cyr (2000), Interplanetary acceleration of coronal mass ejections, *Geophys. Res. Lett.*, *27*(2), 145–148, doi:10.1029/1999GL003639.

Gopalswamy, N., A. Lara, S. Yashiro, M. L. Kaiser, and R. A. Howard (2001), Predicting the 1-AU arrival times of coronal mass ejections, *J. Geophys. Res.*, *106*, 29,207–29,217, doi:10.1029/2001JA000177.

Gopalswamy, N., S. Yashiro, and S. Akiyama (2007), Geoeffectiveness of halo coronal mass ejections, *J. Geophys. Res.*, *112*, A06112, doi:10.1029/2006JA012149.

Gopalswamy, N., S. Yashiro, G. Michalek, G. Stenborg, A. Vourlidas, S. Freeland, and R. Howard (2009), The SOHO/LASCO CME Catalog, *Earth Moon Planets*, *104*, 295–313, doi:10.1007/s11038-008-9282-7.

Jackson, B. V., M. M. Bisi, P. P. Hick, A. Buffington, J. M. Clover, and W. Sun (2008), Solar Mass Ejection Imager 3-D reconstruction of the 27–28 May 2003 coronal mass ejection sequence, *J. Geophys. Res.*, *113*, A00A15, doi:10.1029/2008JA013224. [Printed *114*(A3), 2009.]

Jian, L. K., C. T. Russell, J. G. Luhmann, R. M. Skoug, and J. T. Steinberg (2008), Stream interactions and interplanetary coronal mass ejections at 0.72 AU, *Sol. Phys.*, *249*, 85–101, doi:10.1007/s11207-008-9161-4.

Kilpua, E. K. J., J. Pomoell, A. Vourlidas, R. Vainio, J. Luhmann, Y. Li, P. Schroeder, A. B. Galvin, and K. Simunac (2009), STEREO observations of interplanetary coronal mass ejections and prominence deflection during solar minimum period, *Ann. Geophys.*, *27*, 4491–4503, doi:10.5194/angeo-27-4491-2009.

Lee, C. O., J. G. Luhmann, D. Odstrcil, P. J. MacNeice, I. de Pater, P. Riley, and C. N. Arge (2009), The solar wind at 1 AU during the declining phase of solar cycle 23: Comparison of 3D numerical model results with observations, *Sol. Phys.*, *254*, 155–183, doi:10.1007/s11207-008-9280-y.

Liu, Y., J. A. Davies, J. G. Luhmann, A. Vourlidas, S. D. Bale, and R. P. Lin (2010), Geometric triangulation of imaging observations to track coronal mass ejections continuously out to 1 Au, *Astrophys. J.*, *710*, L82–L87, doi:10.1088/2041-8205/710/1/L82.

Lopez, R. E., S. Hernandez, M. Wiltberger, C.-L. Huang, E. L. Kepko, H. Spence, C. C. Goodrich, and J. G. Lyon (2007), Predicting magnetopause crossings at geosynchronous orbit during the Halloween storms, *Space Weather*, *5*, S01005, doi:10.1029/2006SW000222.

Michałek, G., N. Gopalswamy, A. Lara, and S. Yashiro (2003), A new method for estimating widths, velocities, and source location of halo coronal mass ejections, *Astrophys. J.*, *584*, 472–478, doi:10.1086/345526.

Odstrcil, D., and V. J. Pizzo (1999), Distortion of the interplanetary magnetic field by three-dimensional propagation of coronal mass ejections in a structured solar wind, *J. Geophys. Res.*, *104*, 28,225–28,239, doi:10.1029/1999JA900319.

Odstrcil, D., P. Riley, and X. P. Zhao (2004), Numerical simulation of the 12 May 1997 interplanetary CME event, *J. Geophys. Res.*, *109*, A02116, doi:10.1029/2003JA010135.

Pomoell, J., R. Vainio, and E. K. J. Kilpua (2010), Observation-based analysis of the deflection of a polar crown filament eruption, *AIP Conf. Proc.*, *1216*, 335–338, doi:10.1063/1.3395868.

Pulkkinen, A., T. Oates, and A. Taktakishvili (2010), Automatic determination of the coronal mass ejection model parameters, *Sol. Phys.*, *261*, 115–126, doi:10.1007/s11207-009-9473-z.

Reiner, M. J., A. Vourlidas, O. C. St. Cyr, J. T. Burkepile, R. A. Howard, M. L. Kaiser, N. P. Prestage, and J. L. Bougeret (2003), Constraints on coronal mass ejection dynamics from simultaneous radio and white-light observations, *Astrophys. J.*, *590*, 533–546, doi:10.1086/374917.

Riley, P., J. A. Linker, Z. Mikic, R. Lionello, S. A. Ledvina, and J. G. Luhmann (2006), A comparison between global solar magnetohydrodynamic and potential field source surface model results, *Astrophys. J.*, *653*, 1510–1516, doi:10.1086/508565.

Schwenn, R., A. Dal Lago, E. Huttunen, and W. D. Gonzalez (2005), The association of coronal mass ejections with their effects near the Earth, *Ann. Geophys.*, *23*, 1033–1059, doi:10.5194/angeo-23-1033-2005.

Shen, C., Y. Wang, J. Zhang, P. Ye, and S. Wang (2009), The kinematic evolution of the 2007 October CME in the inner corona, *Bull. Am. Astron. Soc.*, *41*, 856.

St. Cyr, O. C., et al. (2000), Properties of coronal mass ejections: SOHO LASCO observations from January 1996 to June 1998, *J. Geophys. Res.*, *105*, 18,169–18,185, doi:10.1029/1999JA000381.

Taktakishvili, A., M. Kuznetsova, P. MacNeice, M. Hesse, L. Rastaätter, A. Pulkkinen, A. Chulaki, and D. Odstrcil (2009), Validation of the coronal mass ejection predictions at the Earth orbit estimated by ENLIL heliosphere cone model, *Space Weather*, *7*, S03004, doi:10.1029/2008SW000448.

Taktakishvili, A., P. MacNeice, and D. Odstrcil (2010), Model uncertainties in predictions of arrival of coronal mass ejections at Earth orbit, *Space Weather*, *8*, S06007, doi:10.1029/2009SW000543.

Taktakishvili, A., A. Pulkkinen, P. MacNeice, M. Kuznetsova, M. Hesse, and D. Odstrcil (2011), Modeling of coronal mass ejections that caused particularly large geomagnetic storms using ENLIL heliosphere cone model, *Space Weather*, *9*, S06002, doi:10.1029/2010SW000642.

Temmer, M., S. Preiss, and A. M. Veronig (2009), CME projection effects studied with STEREO/COR and SOHO/LASCO, *Sol. Phys.*, *256*, 183–199, doi:10.1007/s11207-009-9336-7.

Vennerstrom, S., N. Olsen, M. Purucker, M. H. Acuña, and J. C. Cain (2003), The magnetic field in the pile-up region at Mars, and its variation with the solar wind, *Geophys. Res. Lett.*, *30*(7), 1369, doi:10.1029/2003GL016883.

Vršnak, B., D. Sudar, D. Ruždjak, and T. Žic (2007), Projection effects in coronal mass ejections, *Astron. Astrophys.*, *469*, 339–346, doi:10.1051/0004-6361:20077175.

Vršnak, B., T. Žic, T. V. Falkenberg, C. Möstl, S. Vennerstrom, and D. Vrbanec (2010), The role of aerodynamic drag in propagation of interplanetary coronal mass ejections, *Astron. Astrophys.*, *512*, A43, doi:10.1051/0004-6361/200913482.

Wang, Y., C. Shen, S. Wang, and P. Ye (2004), Deflection of coronal mass ejection in the interplanetary medium, *Sol. Phys.*, *222*, doi:10.1023/B:SOLA.0000043576.21942.aa.

Wang, Y., X. Xue, C. Shen, P. Ye, S. Wang, and J. Zhang (2006), Impact of major coronal mass ejections on geospace during 2005 September 7–13, *Astrophys. J.*, *646*, 625–633, doi:10.1086/504676.

Wei, F., and M. Dryer (1991), Propagation of solar flare-associated interplanetary shock waves in the heliospheric meridional plane, *Sol. Phys.*, *132*, 373–394, doi:10.1007/BF00152294.

Yashiro, S., N. Gopalswamy, G. Michałek, O. C. St. Cyr, S. P. Plunkett, N. B. Rich, and R. A. Howard (2004), A catalog of white light coronal mass ejections observed by the SOHO spacecraft, *J. Geophys. Res.*, *109*, A07105, doi:10.1029/2003JA010282.

Yashiro, S., S. Akiyama, N. Gopalswamy, and R. A. Howard (2006), Different power-law indices in the frequency distributions of flares with and without coronal mass ejections, *Astrophys. J.*, *650*, L143–L146, doi:10.1086/508876.

Xie, H., L. Ofman, and G. Lawrence (2004), Cone model for halo CMEs: Application to space weather forecasting, *J. Geophys. Res.*, *109*, A03109, doi:10.1029/2003JA010226.

Zhao, X. P., S. P. Plunkett, and W. Liu (2002), Determination of geometrical and kinematical properties of halo coronal mass ejections using the cone model, *J. Geophys. Res.*, *107*(A8), 1223, doi:10.1029/2001JA009143.

D. A. Brain, G. Delory, and D. L. Mitchell, Space Sciences Laboratory, University of California, 7 Gauss Way, Berkeley, CA 94720, USA. (brain@ssl.berkeley.edu; gdelory@ssl.berkeley.edu; mitchell@ssl.berkeley.edu)

T. V. Falkenberg and S. Vennerstrom, National Space Institute, Danish Technical University, DK-2800 Lyngby, Denmark. (tvf@space.dtu.dk; sv@space.dtu.dk)

D. Odstrcil, A. Pulkkinen, and A. Taktakishvili, NASA Goddard Space Flight Center, Code 674, Greenbelt, MD 20771, USA. (dusanod@gmail.com; antti.a.pulkkinen@nasa.gov; aleksandre.taktakishvili-1@nasa.gov)